Eindhoven University of Technology

MASTER

Simulation of process intensified fatty acid nitrilation in a reactive distillation column

Sagir, Sare

Award date:
2023

Link to publication

Department of Chemical Engineering and Chemistry
Sustainable Process Engineering
Chemical Reactor Engineering Group

Simulation of process intensified fatty acid nitrilation in a reactive distillation column

Master thesis

Sare Sagir
1504738

Graduation supervisor:
Prof. dr. ir. John van der Schaaf

Project supervisor:
ir. Carola Raffel

Advising committee members:
dr. ir. Ivo Roghair
dr. ir. Amin Delparish

Eindhoven, December 8, 2022

Acknowledgements

I would like to thank the following people for helping with this research project:

I would like to express my gratitude to my daily supervisor, ir. Carola Raffel, who guided me throughout this master's project.

My graduation supervisor, prof. dr. ir. John van der Schaaf, for the feedback and advice during the monthly meetings.

To my graduation committee, prof. dr. ir. John van der Schaaf, ir. dr. Ivo Roghair, and ir. dr. Amin Delparish, I am grateful for your attendance during my defense.

The PhD candidates, ir. Zançat Şahin and ir. Brandon Leal Perez, who have helped me with problems in Aspen Plus.

My friends and other master students from the Broeikas and of course my family who supported me and offered deep insight into the study.

Abstract

Sustainability has been a growing global concern in recent years because of climate change. Greener chemistry and energy efficiency in industrial processes can be obtained by using less hazardous chemicals.[1] Fatty acids, such as oils and fats, are renewable. They deserve special attention because they appear in industrial-waste streams.[2,3] During the nitrilation of fatty acids, the fatty acid reacts with ammonia to form amide and water. This amide can then dehydrate to obtain the desired product, nitrile and water. Fatty nitriles can be used in the pharmaceutical and polymer industries.[4] The second reaction is enhanced by the presence of a dehydration catalyst, for example, ZnO or Al_2O_3.[4] For each mole of nitrile, two moles of water are formed.

In industry, the fatty acid nitrilation is carried out in a semi-batch reactor with an excess of NH_3 that is needed to remove the water produced in the reaction to move the reaction equilibrium to the product side.[5] To bring the reaction to completion, it is necessary to shift the reaction equilibrium to the right-hand side. This is complicated by the formation of two moles of water per mole of nitrile. Thus, process intensification is needed.

This study has aimed to determine how fatty acid nitrilation can be intensified using an innovative reactor concept. Experiments are done to determine the quality of the kinetics available in the literature. Different process configurations are proposed and evaluated, these simulations are supplemented by the kinetic data that can most accurately describe the experimental results. Then the best process configuration is simulated more in-depth. Finally, the most promising process configuration is compared to the semi-batch benchmark and evaluated if the goal is reached.

From the experimental part, it can be concluded that the reaction from amide to nitrile is reversible. The obtained mean equilibrium composition is 12.0 % acid, 50.2 % amide and 37.8 % nitrile. Thus, the reaction equilibria favor the production of the amide and nitrile sides of the two reactions respectively. Moreover, batch simulations have shown that the best fit to the experimental data was obtained with the equilibrium constant determined from Density-functional theory (DFT) by using kinetic data of Mekki-Berrada et al. The findings of the study of the different process configurations resulted that reactive distillation was the best for in-situ water removal. However, only 38 % yield to nitrile was obtained in the reactive distillation. So, the reactive distillation was not suitable at this reaction time - because more residence time was needed for the slow reaction of amide to nitrile. Therefore, the optimized design was a reactive distillation column followed by a Continuous stirred tank reactor (CSTR).

All in all, this model was made more efficient by adding a reduced excess of ammonia, purifying the outcome streams and recycling acid and amide back to the model, resulting in an overall 98 % conversion of acid, 0 % yield to amide, 98 % yield to nitrile and 100 %. All acid that was present in the model was converted, so there was a mass loss of 2 %.

Contents

List of Figures

List of Tables

List of Abbreviations

A   after

B   before

CAGR Compound Annual Growth Rate

CSTR Continuous stirred tank reactor

DFT   Density-functional theory

IS   internal standard

L-DIST liquid distillate

NMR Nuclear magnetic resonance

NRTL Non-Random Two Liquid

PROD product stream

RDC   Reactive distillation column

RPM   revolutions per minute

RTD   residence time distribution

STY   space-time yield

TBR   Trickle bed reactor

V-DIST vapor distillate

VLE   Vapor-Liquid Equilibrium

1 Introduction

Sustainability has been a growing global concern in recent years because of climate change. Greener chemistry and energy efficiency in industrial processes can be obtained by using less hazardous chemicals.[1] But fatty acids are not used because they are less hazardous than petroleum, but because they are renewable. Therefore, fatty acids, such as oils and fats, deserve special attention because they appear in industrial-waste streams.[2,3] These acids can be reacted to give fatty nitriles, an important base chemical.

Fatty nitriles can be used in various applications. These nitriles are platform molecules that can be used in the pharmaceutical and polymer industries.[4] For example, the hydrogenation of nitriles can lead to the production of primary amines, which can be converted into surfactants. Furthermore, nitriles can be used in the field of renewable energy resources and can be converted into biofuels and fine chemicals.[4] Because of their high energy density, they are investigated as aviation fuels.[11]

During the nitrilation of fatty acids, the fatty acid reacts with ammonia to form amide and water. This amide can then dehydrate to obtain the desired product, nitrile and water. The second reaction is enhanced by the presence of a dehydration catalyst, for example, ZnO or Al_2O_3.[4] For each mole of nitrile, two moles of water are formed.

The fatty acid nitrilation can be operated in liquid or gas phases, it is operated in the industry in these ways. The reaction temperature for the liquid phase is between 200 and 300 °C and for the gas phase between 300 and 450 °C.[3,4] In liquid-phase reactions, only ammonia and water is in the gas phase. At the gas phase conditions, fatty acids would also be vaporized. The gas phase reaction is faster (10 seconds until full conversion of acid to nitrile), but it has a lower selectivity towards the nitrile.[11] The liquid phase reaction is slower (5-12 hours until full conversion), but it has a higher selectivity towards the nitrile.[3–5] There are fewer side reactions in the liquid phase and more side reactions in the gas phase, due to higher temperatures and the start of cracking the carbon chain.[3] Since there are more side reactions in the gas phase - it is more favorable to have high selectivity towards nitrile. Thus, the project focus is on liquid phase nitrilation.

In industry, the fatty acid nitrilation is carried out in a semi-batch reactor with an excess of NH_3 that is needed to remove the water produced in the reaction to move the reaction equilibrium to the product side.[5] To bring the reaction to completion, it is necessary to shift the reaction equilibrium to the right-hand side. This is complicated by the formation of two moles of water per mole of nitrile. Thus, the process can be intensified by using a reactor with in-situ water removals, such as a reactive distillation column or a trickle bed reactor. Process intensification can be achieved by improving the process without offering product quality. This can be obtained by improving yield and selectivity, fewer wastes, lowering operating costs and improving safety.

This study has aimed to determine how fatty acid nitrilation can be intensified using an innovative reactor concept. Experiments are done to determine the quality of the kinetics available in the literature. Different process configurations are proposed and evaluated, these simulations are supplemented by the kinetic data that can most accurately describe the

experimental results. Then the best process configuration is simulated more in-depth. Finally, the most promising process configuration is compared to the semi-batch benchmark and evaluated if the goal is reached.

2 Theoretical Background

2.1 Fatty amine market

In the future, the use of free fatty acids from renewable resources would be a promising feedstock for the production of chemicals and fuels as long as there is a growing demand, especially in the fatty amines market.[12] Fatty amines are projected to grow from USD 2.9 billion in 2019 to USD 4.0 billion in 2024, at a Compound Annual Growth Rate (CAGR) of 6.5 %, between 2019 and 2024.[13] As they are often produced from nitriles, the production of nitriles is also important.

2.2 Fatty acid nitrilation

Fatty acid nitrilation consists of two reactions. The first reaction is a reversible amidification reaction, where one mole ammonia and one mole carboxylic acid react to form one mole amide and one mole water.[3,4] Subsequently, a reversible nitrilation takes place from one mole amide to obtain one mole of desired product nitrile and one mole of water.[3] These two reactions are shown in Figure 1, where R is $CH_3(CH_2)_n$ for fatty acids containing C_8 to C_{18} chains.
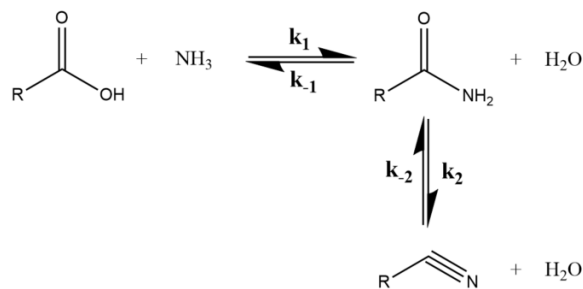
Figure 1: Schematic overview of the fatty acid nitrilation; fatty acid reacts with ammonia to amide, amide dehydrates to nitrile and water.

In literature, three different routes are known of the conventional nitrile process: the batch process, the gas-phase continuous process and the liquid-phase (semi-)batch process. In batch processes, due to high temperatures - side reactions can occur in the presence of unsaturated fatty acids such as isomerization, polymerization, oxidation, trimerization etc.[3] Furthermore, it is not possible to feed a stoichiometric amount of gaseous ammonia to the acid all at once in the batch process - in contrary of continuous processes. The second advantage of processing continuously is to prevent the formation of side products. Thus, the yield of nitrile would increase.

Nitrile continuous processes involve gas-phase reactions of fatty acids with ammonia at a temperature range between 300 and 450 °C in the presence of a solid catalyst bed.[3,4] Side reactions are caused by high temperatures and short reaction time (few seconds) between acid and ammonia. Furthermore, polymerization/dimerization of the fatty acid or nitriles could be prevented due to the greater distance between molecules. An advantage of this gas-phase process is that no catalyst recovery is needed since a heterogeneous catalyst is used in a solid or liquid phase.[3] Shirazi et al. prevented cracking or polymerization by the

combination of lower reaction temperature (400 °C) and short residence time (10 s), while the ammonia in excess (2-4 times the required stoichiometric value) is fed at room temperature.

Lastly, the conventional semi-continuous process is in the liquid phase, where the fatty acid is fed once with a homogeneous catalyst in the beginning. Second, the ammonia is fed continuously. Figure 2 shows the semi-batch process in the liquid phase.[5] The reaction begins when the ammonia feed is started. The product nitrile is formed and remains in the liquid phase. A vapor phase is also formed, essentially containing water, ammonia and unreacted fatty acids which were vaporized via the vent, flowing to the gaseous circuit to prevent feed losses. The unreacted fatty acid is removed from the water and ammonia by one-step distillation and is recycled back into the reactor. Then the ammonia is removed from the water and also recycled back into the reactor. By continuously adding ammonia and removing gasses from the reactor, the nitrile production was improved by Mekki-Berrada et al.[5,11] However, a condenser is used for removing the water. Since the process is carried out in a batch reactor, this would have caused a slow reaction. Thus, there a is need for process optimization of fatty acid nitrilation.
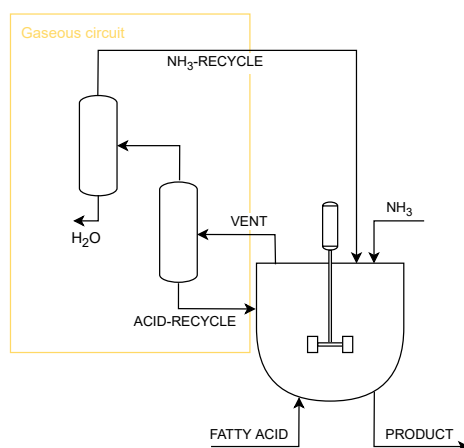
Figure 2: Schematic overview of conventional nitrile process operating in liquid phase[4,5]

Mekki-Berrada et al. studied the fatty acid nitrilation in a batch process using heterogeneous, homogeneous or without catalysts. The experiments without catalyst were done in an open batch system, including the demister which removes water. At 300 °C an equilibrium appears to be found to be 5:15:80 composition of acid, amide and nitrile, respectively, though it was not confirmed whether the system was truly in equilibrium, as ammonia continued to be fed into the system. The mole compositions over time are shown in Figure 3a. The experiments were carried out in the semi-batch, where the acid was fed at the beginning and the NH_3 was fed continuously at a flow rate of 3 g h^{-1} with an excess of 2.3 times the required stoichiometric value for 8 h. The reaction order from acid toward the amide side was found to be approximately 1. Moreover, the reaction rate constant k_2 was found to be dependent on the present catalyst. Different catalysts were tested such as metal oxides, where the most efficient catalyst was found to be zinc oxide (homogeneous) by achieving the highest nitrile conversion. Mekki-Berrada et al. obtained almost 100 % conversion with 0.23 mol % ZnO catalyst at 300 °C. Figure 3b shows the mole compositions of acid, amide and nitrile over time

4

by using a 0.23 mol % ZnO catalyst at different temperatures.
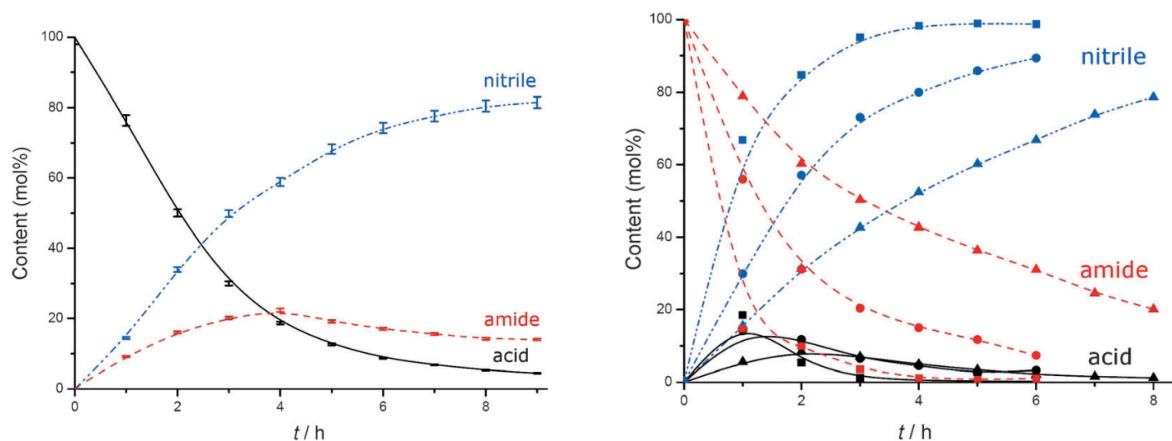
(a) Nitrilation without catalyst at 300 °C in a semi-batch process

(b) Nitrilation with catalyst at 250 (▲), 275 (●) and 300 °C (■) in a semi-batch process

Figure 3: Contents of acid (black), amide (red) and nitrile (blue) over time.[4]

The liquid phase nitrilation is researched for the kinetics by Bizhanov et al. in a packed bed flow reactor using a stationary catalyst aluminum oxide. A mixture of C_{10}-C_{22} aliphatic acids is used for direct reaction with ammonia at 300 °C. The almost full conversion is obtained after a reaction time of 2 h achieving 98 % yield to nitrile. The formation of amide and nitrile are obtained in the zero order, where the reaction rate constants were found to be 7.4 and 5.86 mol min^{-1}, respectively. Since the nitrilation is processed at temperatures of 300 °C and above, Bizhanov et al. found out that the formation of ammonium salts in the side reaction (see Figure 4), fatty acids reacting with ammonia to form an ammonium salt and amide at a temperature below 300 °C, is negligible because only small amounts were obtained after 9 h.[14] Therefore, the formation of ammonium salts are not taken into account in this study.
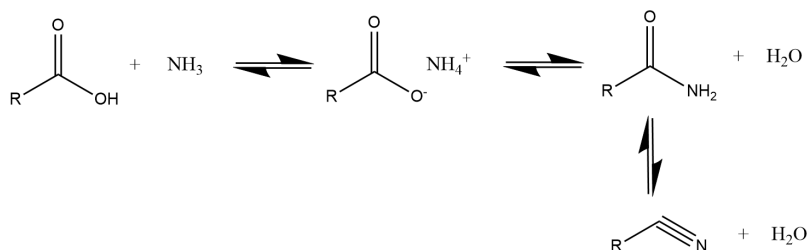
Figure 4: Schematic overview of the fatty acid nitrilation; fatty acid reacts with ammonia to amide, amide dehydrates to nitrile and water.

Table 1 shows an overview of different conditions where the nitrilation process is in liquid and gas phases.

5

Table 1: Conditions of nitrilation process in liquid and gas phases.[3,4]

	Liquid phase	Gas phase
Reaction temperature [°C]	200 - 300	300 - 450
Reaction time	5-12 h	10 s
Selectivity to nitrile	High	Low
Side reactions	Few	More

2.2.1 Reaction mechanism and kinetics

The reaction kinetics of the fatty acid nitrilation in the liquid phase have not been researched extensively. This is described in one paper, which is Mekki-Berrada et al. Another research from Mekki-Berrada et al. were experiments performed on the hydration of nitrile with and without ZnO catalyst at 250 °C. It has been found that no formation of amide was observed and concluded that the reaction from amide to nitrile and water is irreversible. No reversibility means that the water formation in the process does not affect the second reaction because all amide can be converted toward the nitrile. On the contrary, amide can react back to acid with the present water in the process - which is improved by using an excess of ammonia. Moreover, the second reaction was also forced by the instability of water in the medium. Finally, the reaction rate constants were obtained at 300 °C and are shown in Table 2.

Table 2: Activation energy and pre-exponential factors obtained by Mekki-Berrada et al. for the reversible reaction of acid to amide and irreversible reaction from amide to nitrile.[4]

Reaction	Activation energy [kJ mol^{-1}]	Pre-exponential factor [s^{-1}]
k_1	85	62190
k_{-1}	85	7720
k_2	85	12867

Different studies from the Eindhoven University of Technology researched the kinetics of fatty acid nitrilation. First, Appelman researched a closed wall-coated microcapillary reactor with a γ-alumina catalyst for the nitrilation reaction.[6] Several ways were studied to improve the coating stability. The microcapillary reactor is found to have higher reaction rates than a conventional batch reactor, which is increased further by the use of a γ-alumina catalyst. Moreover, Figure 5 shows the obtained results where the concentrations of acid, amide and nitrile are demonstrated over time. Table 3 presents the pre-exponential factor and activation energy, which was obtained for each kinetic rate constant in the microcapillary reactor. Moreover, the reaction from amide to nitrile was observed to be only forward.[6]
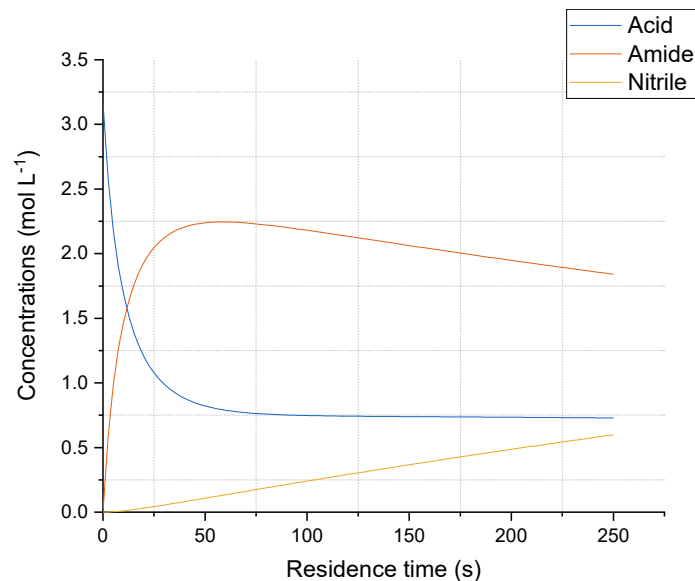
Figure 5: Obtained results from Appelman; Concentrations of acid, amide and nitrile in mol L^{-1} over residence time in s. [6]

Table 3: Activation energy and pre-exponential factors obtained by Appelman for the reversible reaction of acid to amide and irreversible reaction from amide to nitrile. [6]

Reaction	Activation energy [kJ mol^{-1}]	Pre-exponential factor [s^{-1}]
k_1	36.3	18.6
k_{-1}	29.9	81.1
k_2	135.4	$2.494 \cdot 10^9$

Secondly, Verdonk researched the same set-up as Appelman but focused on different parameters, such as the influence of the pressure and the influence of the ratio of ammonia and acid on the fatty acid nitrilation. [7] Increasing the pressure would decrease the nitrile formation and adding more ammonia than the required stoichiometric value would not influence the nitrile concentration. Moreover, the obtained results of Verdonk are shown in Figure 6 where the concentrations of acid, amide and nitrile are demonstrated over time. The following kinetic constants could be fitted to the experimental data without the catalyst in Table 4 and with the catalyst in Table 5, where the reaction from amide to nitrile is considered irreversible. [7]
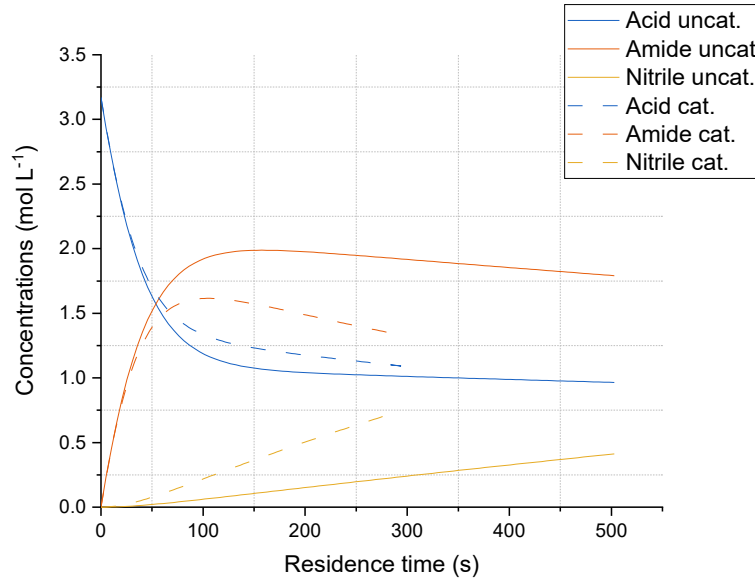
Figure 6: Obtained results of catalyzed and uncatalyzed processes from Verdonk; Concentrations of acid, amide and nitrile in mol L^{-1} over residence time in s.[7]

Table 4: Activation energy and pre-exponential factors obtained by Verdonk without catalyst for the reversible reaction of acid to amide and irreversible reaction from amide to nitrile.[7]

Reaction	Activation energy [kJ mol^{-1}]	Pre-exponential factor [s^{-1}]
k_1	67.1	$3.09 \cdot 10^5$
k_{-1}	162.8	$4.73 \cdot 10^{15}$
k_2	159.6	$1.86 \cdot 10^{11}$

Table 5: Activation energy and pre-exponential factors obtained by Verdonk with catalyst for the reversible reaction of acid to amide and irreversible reaction from amide to nitrile.[7]

Reaction	Activation energy [kJ mol^{-1}]	Pre-exponential factor [s^{-1}]
k_1	16.5	8.52
k_{-1}	183.7	$1.37 \cdot 10^{18}$
k_2	136.6	$4.66 \cdot 10^9$

The kinetic rate constants from the research of Mekki-Berrada, Appelman and Verdonk are compared in Table 6 at a temperature of 300 °C. As can be seen, the kinetic rate constants of Verdonk and Appelman - both obtained in a closed system - are faster than that from Mekki-Berrada et al. obtained in an open system. The backward reaction from amide to acid is a lot faster for Appelman and Verdonk than for Mekki-Berrada et al. Furthermore, Verdonk has obtained faster kinetic rate constants for the reversible reaction of acid to amide compared with Appelman. The rate constants are similar for the second forward reaction from amide to

nitrile, however, the rate constant is slower at Verdonk when no catalyst is used in the system.

Table 6: Kinetic rate constants obtained by Mekki-Berrada et al., Appelman and Verdonk at a temperature of 300 °C. [4,6,7]

Data	k_1 [s^{-1}]	k_{-1} [s^{-1}]	k_2 [s^{-1}]
Mekki-Berrada	$1.11 \cdot 10^{-3}$	$1.38 \cdot 10^{-4}$	$2.29 \cdot 10^{-4}$
Appelman	$9.12 \cdot 10^{-3}$	0.15	$1.12 \cdot 10^{-3}$
Verdonk without catalyst	0.236	6.82	$5.25 \cdot 10^{-4}$
Verdonk with catalyst	0.267	24.5	$1.64 \cdot 10^{-3}$

2.2.2 Chemical equilibrium

A general equilibrium reaction is shown in Equation 2.1, involving components A, B, C and D, with their stoichiometric coefficients a, b, c and d.

$$aA + bB \rightleftharpoons cC + dD \tag{2.1}$$

Chemical reactions could be moved towards the left side, to the right side, or be in a state of equilibrium, depending on initial conditions. [15] They are in equilibrium in which reactants and products are present, but have no more tendency to change. [16] An equilibrium-limited reaction means that the equilibrium appears faster than the kinetic rates can bring the reaction to completion. On the contrary, a kinetically limited equilibrium reaction means that the kinetics are faster than that the equilibrium appears.

At constant temperature and pressure, Gibbs free energy can be used to determine the maximum amount of work carried out in a closed system. Equation 2.2 shows the Gibbs free energy change

$$\Delta G = \Delta H - T \Delta S \tag{2.2}$$

where T is the temperature in K, ΔG the change in Gibbs free energy in J, ΔH the change in enthalpy in J and ΔS the change in entropy in J K^{-1} between the reactants and products. [15] Enthalpy is a measure of the net energy during a chemical reaction and entropy is a measure of disorder. The Gibbs free energy can also be defined as follows

$$\Delta G = \Delta G^\circ + RT \, ln \, Q \tag{2.3}$$

where R is the gas constant in J mol^{-1}K^{-1}, ΔG° the change in Gibbs free energy at standard conditions (298 K; 1 atm) and Q the reaction quotient that defines the activities of products towards the activities of reactants. Equation 2.4 shows the reaction quotient for reaction 2.1, where the terms in brackets are the molar concentrations of the reactants and products to the power to its stoichiometric coefficient a, b, c and d.

$$Q = \frac{[C]^c [D]^d}{[A]^a [B]^b} \tag{2.4}$$

At equilibrium ΔG is zero, Equation 2.3 can be simplified to

$$\Delta G^\circ = -RT \, ln \, K_{eq} \tag{2.5}$$

where K is the equilibrium constant that can define the equilibrium position of the reaction. Equation 2.4 can be further simplified to

$$K_{eq} = \frac{[C]^c[D]^d}{[A]^a[B]^b}$$ (2.6)

where the subscript 'eq' indicates that the concentrations are at equilibrium.

Equation 2.6 is filled in for the two reactions of the fatty acid nitrilation (Figure 1 in Equations 2.7 and 2.8

$$K_{eq,1} = \frac{[RCONH_2][H_2O]}{[RCOOH][NH_3]} = \frac{k_1}{k_{-1}}$$ (2.7)

$$K_{eq,2} = \frac{[RCN][H_2O]}{[RCONH_2]} = \frac{k_2}{k_{-2}}$$ (2.8)

where k_1, k_{-1}, k_2 and k_{-2} are the kinetic rate constants in s^{-1}. All components have a stoichiometric value of 1 - this is negligible in the formula. The kinetic rate constant can be expressed with the Arrhenius equation

$$k = k_0 e^{\frac{-E_a}{RT}}$$ (2.9)

where k_0 is the pre-exponential factor in the same unit as k, E_a is the activation energy in J mol^{-1}, R is the gas constant in J $mol^{-1}K^{-1}$ and T is the temperature in K.

Moreover, equalizing the Equations 2.2 and 2.5 give the van 't Hoff equation:

$$lnK_{eq} = \frac{-\Delta H}{R}\frac{1}{T} + \frac{\Delta S}{R}$$ (2.10)

Chila from the Eindhoven University of Technology researched the fatty acid nitrilation with the fatty amide as starting reactant in a closed small batch reactor. Influences of different parameters such as temperature, water addition and ammonia addition were tested to see the effects on the process and derive the chemical equilibrium constants. Chila reached an equilibrium of 25 mol % of nitrile, 70 mol % of amide and 5 mol % of acid by using 5 % headspace in the process. This concluded that the second reaction from amide to nitrile and water is reversible.[8] Figure 7 shows the obtained fitted line relations on the *ln K* values over *1/T* for different headspace percentages in the van 't Hoff graph.
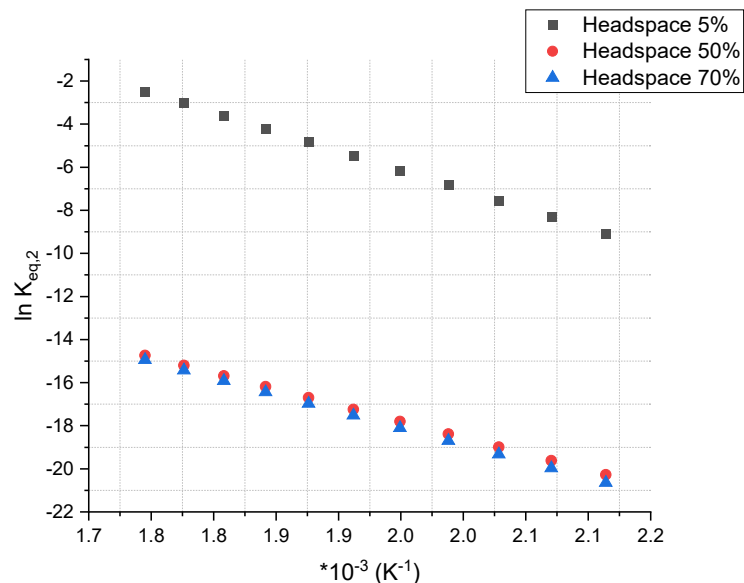
Figure 7: The van 't Hoff graph for different headspace percentages.[8]

The research from Chila is in contrast with the findings and resulting kinetic models from Mekki-Berrada et al., Appelman and Verdonk. They observed little to no backward reaction of nitrile to an amide.[4,6,7] It is possible that the back reaction is slow and needs specific reaction conditions to be observable. Unlike Mekki-Berrada et al., Appelman and Verdonk, Chila worked in a closed batch system which could develop high autogenic pressures. Furthermore, the reaction times were longer than for Appelman and Verdonk and the water was not removed from the reaction as with Mekki. This could lead to the nitrile hydrolysis reaction being observed in Chila's case.

Through another research, the equilibrium constant was determined by the DFT method by using the Gibbs free energy from Equation 2.2 and using the enthalpies and entropies for both reactions from Table 20 in Appendix A.I.[9] Furthermore, implementing these calculated Gibbs free energies in Equation 2.5 would give the equilibrium constant for the reaction from acid to amide (Figure 8a) and the reaction from amide to nitrile (Figure 8b) in a temperature range from 200 to 300 °C.
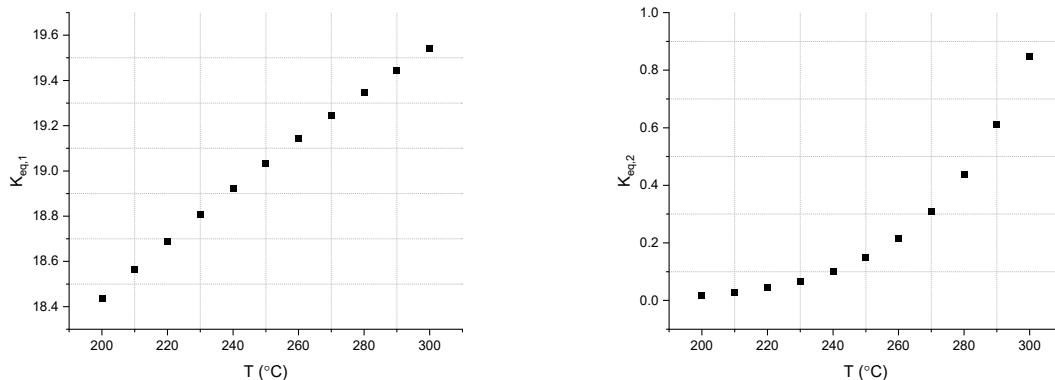
(a) Equilibrium constant for the first reaction   (b) Equilibrium constant for the second reaction

Figure 8: Equilibrium constants obtained from DFT data for the first reaction acid to amide and second reaction amide to nitrile.[9]

Overall, three studies found that the second reaction of the fatty acid nitrilation from amide to nitrile and water is irreversible. On the contrary, one research has obtained results that show the equilibrium composition and so the reversibility of the second reaction. The second reaction will be debatable as an equilibrium reaction. In chemistry, the mechanism of the hydrolysis of nitrile to amide catalyzed by an acid or base is known. In the case that the process is catalyzed by the acid, the nitrile becomes protonated. The electrophilicity of nitrile can be increased by the protonation. Moreover, the nitrile accepts water hereafter a proton transfer takes place. Finally, deprotonation takes place where an amide and water are formed by using acid as a catalyst. Interestingly, the fatty acid nitrilation process contains an acid, the fatty acid, which can provide the hydrolysis of the nitrile.[17]

This study focused on a specific kinetic model for the fatty acid nitrilation, where it is assumed that there is no formation of ammonium salts:

$$r_1 = k_1 C_{RCOOH} C_{NH_3} \tag{2.11}$$

$$r_{-1} = k_{-1} C_{RCONH_2} C_{H_2O} \tag{2.12}$$

$$r_2 = k_2 C_{RCONH_2} \tag{2.13}$$

$$r_{-2} = k_{-2} C_{RCN} C_{H_2O} \tag{2.14}$$

where C_i is the concentration in mol L^{-1} for component i.

2.3 Process intensified reactors

The conventional process has been discussed for fatty acid nitrilation. Several process designs can be used to intensify this process. In the conventional process, only ammonia was in continuous flow but with a CSTR, a Trickle bed reactor (TBR) and a Reactive distillation

column (RDC) all streams are continuous. These reactors are always operated at a steady state and are suitable for gas-liquid-solid reactions.[18] An advantage of continuous processes is their high capacity and better product quality.[19] Continuous systems are more economic, it can be easily achieved to recover sensible heat from the reactor effluent at high temperatures, where sensible heat is the amount of heat that is needed to change the temperature of a system instead of changing its phase. Moreover, they are less labor intensive. A major advantage would be the reduction in the amount of produced waste streams that result in higher yield.[20]

2.3.1 Continuous stirred tank reactor

A commonly used reactor in industrial processes is the CSTR, primarily used for liquid reactions and is assumed to have perfect mixing.[18] The residence time distribution (RTD) of a CSTR is an important feature of the mixing that occurs in the reactor, which is defined as the distribution of time that the molecules exiting a reactor have spent inside the reactor.[21] The RTD could affect the performance of the CSTR and on the selectivity of the desired product. Furthermore, every point in the reactor is assumed to have the same value, such as the temperature or concentration, which comes from the assumption of perfect mixing within the reactor.[19] Figure 9 shows a schematic overview of a CSTR, where the reactants are continuously fed and the products are continuously withdrawn. This system is well suited for slow reactions and can accommodate residence times greater than one hour.[19]
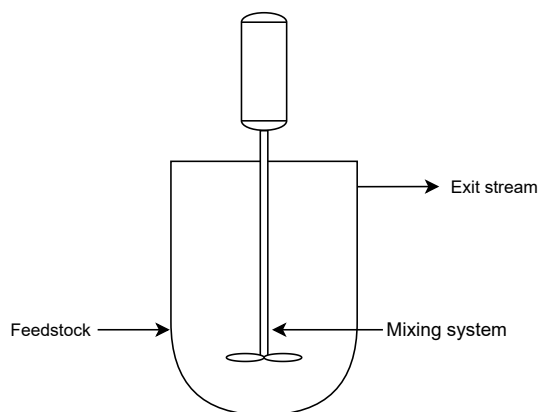
Figure 9: Schematic overview of a continuous stirred tank reactor with a feed and exit stream.

2.3.2 Trickle bed reactor

The trickle bed reactor is a specific type of packed bed reactor. In this reactor, large amounts of catalysts can be used with large particle diameters. Figure 10 shows a schematic view of the process, where the reactant the in liquid phase flows downwards and the gas flows upwards. In this case, it is called counter-current flow in the process. When the gas flows also downwards, there is co-current flow in the process. When the liquid flows upwards, it is not a trickle bed reactor.[19] The TBR is suitable for in-situ water removal.
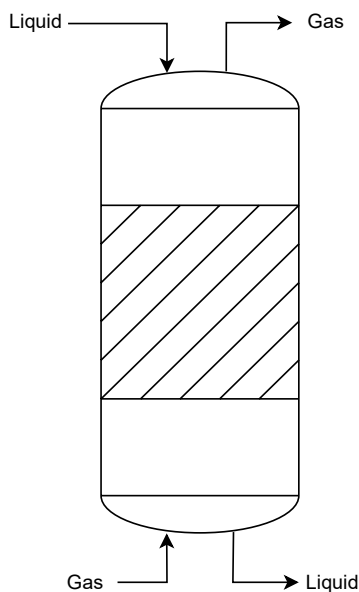
Figure 10: Schematic overview of a trickle bed reactor.

The advantages of a TBR are that it is a simple design, cheap and ideal for slow reactions. The second advantage is that there are no moving parts. There is no catalyst abrasion. Large reactors - heights up to 30 m - are possible and it is also possible to operate at high pressure. On the contrary, there are disadvantages of the TBR such as pressure drop, mass transfer to and from the catalyst and heat transfer to and from the reactor. Furthermore, maldistribution could be possible and exchanging the catalyst would be difficult in the reactor.[21]

2.3.3 Reactive distillation column

Reactive distillation, also called catalytic distillation, contains in general, stages in the rectifying, the reactive and the stripping section. Figure 11 shows the schematic view of an RDC. The first stage is always the condenser, and the last stage is the reboiler. The reactants can be fed on the desired stages. Mostly, the heavy product can be fed in the top of the column flowing downwards and the light product from the bottom flowing upwards, so there is a countercurrent flow in the column.[22] From the top of the RDC, the light product can be obtained. The bottom product is the heaviest. The reflux ratio is the ratio of the liquid returned to the column divided by the liquid removed as a product. When the reflux ratio is too low or near zero, it would behave more like a stripping column.
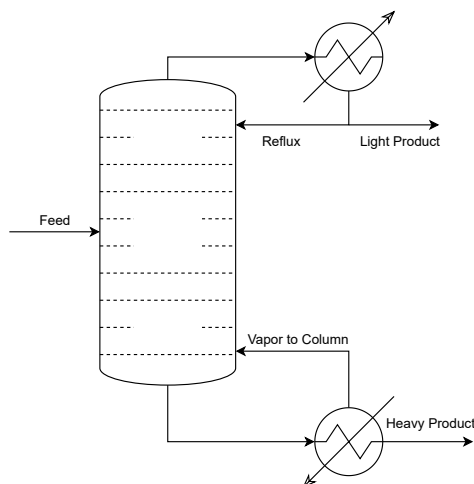
Figure 11: Schematic overview of a reactive distillation.

In the reactive section, several irreversible and reversible reactions can take place such as hydrogenation, hydrodesulfurization, esterification, etherification, heterogeneous catalysis, homogeneous catalysis, thermal (non-catalyst), etc. In most cases, all reactions take place in the liquid phase, but it is conceivable that reactions take place in the gas phase locating the catalyst in the gas phase.[23] Reactive distillation is generally used for performing equilibrium-limited reactions.[24]

The advantages of the RDC are that there is an improved conversion of the reactant, improved selectivity of the desired product and there is avoidance of azeotropes.[25] Moreover, there is reduced formation of the by-product and less catalyst is required for the same conversion.[26] Hot spots and runaways can be avoided by using liquid evaporation as a thermal flywheel. On the contrary, by an improper choice of the feed stage, reflux, amount of catalyst, etc. the RDC is not an advantage anymore.[26]

If the reaction is fast and equilibrium-limited - the required size of the reactive zone is influenced by the contact between the vapor and liquid. For slow reactions, vapor-liquid contact is less important. Small catalyst particles (1-3 mm) need to be used to avoid intra-particle diffusional limitations. A low-pressure drop is needed when the RDC is in counter-current operation with these small particles.[26] This is to prevent uncontrolled pressure drop and flooding. Flooding is when vapor and liquid flow rates are that the drag force is higher in amount or equal to the gravitational force, and as a result that the proper column operation stops.[27] Weeping can also occur when the vapor flow rate is low - a small amount of liquid is flowing from the tray to the lower one through the opening of the tray.

Reactive distillation processes can be operated in packed- or tray columns. The most important part of packed column internals is the packing itself. To allow for mass transfer, the packing needs a large surface area per unit of volume. Moreover, the packing needs to be completely wetted by the liquid. These packings are random- or structured packings. In industry, most packed columns are used with random packings collected with a large amount of specially formed particles. On the contrary, structured packings have a homogeneous bed structure. There is also low-pressure drop because of the vertical orientation of the packings.[26,27]

On the other hand, tray columns contain horizontal trays with perforations. Three principal plates are used as vapor-liquid contacting devices such as the sieve plate, the bubble cap plate and the valve plate. Bubble cap trays are used to prevent leaking downwards through the plate. However, these plates are complex, expensive and have high-pressure drops. On the other hand, sieve plates are more simple, inexpensive and have high separation efficiency at lower pressure drops. The distance between two trays (tray spacing) needs to be small as possible, but large enough so that no liquid reaches the tray above. In industry, a tray spacing from 0.15 to 1.0 m is used, depending on the tray diameter and vapor flow. The height of the column can be defined as [26,27]

$$H_{column} = H_{spacing} N_s \tag{2.15}$$

where $H_{spacing}$ is the tray spacing in m and N_s is the number of stages.

Reactive distillation is an efficient process to intensify the fatty acid nitrilation, containing the chemical reaction and distillation in one column. [22] It is suitable for in-situ water removal, but it can lead to complex interactions between vapor-liquid equilibrium, mass transfer, chemical reaction kinetics and catalyst diffusion. [26,28]

These reactor designs can also be with each other if it is suitable to obtain higher yields of the product.

2.4 Ammonia and water solubility

The solubilities of ammonia and water in fatty acids, amides and nitriles are necessary for modeling. These solubilities are obtained from research in COSMO-RS. [9] Figure 12a shows the solubility for ammonia and Figure 12b for water in a temperature range of 200 to 350 °C. The ammonia solubility in acid is higher than amide and nitrile from 200 to 350 °C. On the other hand, the water solubility is higher in amide than in acid and nitrile.

(a) Ammonia solubility   (b) Water solubility
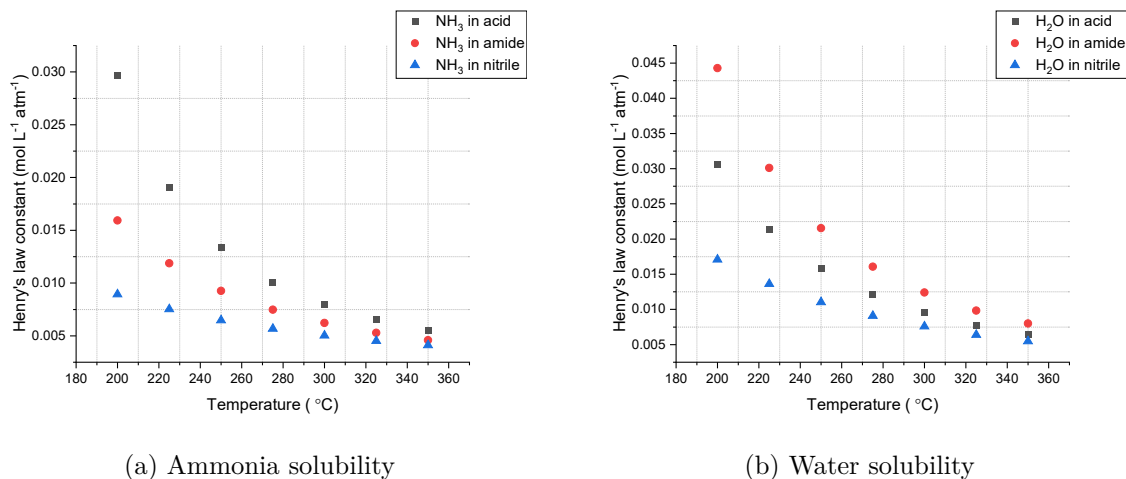
Figure 12: Solubilities in acid, amide and nitrile at a temperature range of 200 to 350 °C.

The solubility can be defined as

$$H = \frac{c_i}{p_i} \tag{2.16}$$

where H is the Henry's law constant in mol L^{-1} atm^{-1}, c is the concentration of component i in mol L^{-1} and p is the partial pressure of component i in atm. The partial pressure can be simplified to the ideal gas law

$$p_i = \frac{n_i RT}{V} \tag{2.17}$$

where n_i is the amount of the component i and V is the volume in m^3.

2.5 NMR spectroscopy

Nuclear magnetic resonance (NMR) spectroscopy is a characterization technique to determine the chemical structure of a molecule. Moreover, it can determine solubility, diffusion potential and phase changes. The experiments are performed on the nuclei of the atoms and not the electrons. The obtained information can be mapped. NMR can be performed in the liquid and solid states.[29]

The NMR spectra give different peaks of the fatty components with an internal standard (IS). These areas can be determined with baseline correction and by using manual integration. A standard internal can be chosen that does not react with the sample components. Moreover, with an internal standard, familiar results can be obtained, since the concentration of this standard is known. After the NMR analysis, the moles can be determined from the desired component

$$n_i = \frac{I_i}{I_{IS}} \frac{N_{IS}}{N_i} n_{IS} \tag{2.18}$$

where n is the mole of the acid, amide, or nitrile and IS, I is the integral of ^{1}H NMR peaks of the desired component i and IS and N is the number of protons of the component i or IS.

3 Materials and Methods

3.1 Experimental

For the batch experiments, fatty compounds were used with C_{12} chains such as Lauric acid (>98% TCI), Lauramide (>96% TCI) and Lauronitrile (>98% TCI). Fatty compounds with C18:1 chains were used for the viscosity measurements and vapor-liquid equilibrium experiments, such as oleic acid (VWR), oleamide (TCI) and oleonitrile (Nouryon). Demi-water is used for each experiment.

3.1.1 Batch experiments

Batch experiments were done in mini-autoclaves with a headspace percentage of 80 % - in order to determine the reversibility (and equilibrium composition) of the reaction from amide to nitrile. The autoclaves had a length of 77.79 mm with caps and an internal diameter of 10.35 mm. These experiments were operated for 5 and 10 h by using a heater and a magnetic stirrer with a diameter of 4 mm and a length of 10 mm. The reactants were nitrile, amide and water. The reactor was charged with acid, amide, nitrile and water for 9 different experiments, see Table 7 for the exact weights and resulting headspace. The compositions are shown in Table 8 where the nitrile and water were at a 1:1 mole ratio. Experiments 7 and 8 were the same experiment as experiments 1 and 6, respectively, but for a longer batch time to see the impact on the reversibility and whether the equilibrium composition had been reached. Experiment 9 was done to see if the presence of acid influences the reversibility of nitrile to an amide.

Table 7: Exact weights of the components amide, nitrile, water and acid used in the autoclave experiments; headspace determined with the exact weights and each experiment has another batch volume.

Experiment	Amide [g]	Nitrile [g]	Water [g]	Acid [g]	Headspace [%]	Batch volume [mL]
1	0.790	0.124	0.013	-	80.0	5.259
2	0.744	0.167	0.019	-	80.0	5.259
3	0.710	0.227	0.021	-	79.7	5.342
4	0.102	0.791	0.076	-	79.7	5.301
5	0.048	0.856	0.081	-	79.7	5.394
6	0	0.879	0.090	-	79.9	5.298
7	0.798	0.126	0.013	-	79.9	5.301
8	0	0.859	0.085	-	80.1	5.226
9	-	0.843	0.083	0.049	79.5	5.275

Table 8: Mole compositions of each component used in the experiments; Experiments 1 to 6 and 9 had a batch time of 5 h; Experiments 7 and 8 had a batch time of 10 h.

Experiments	$x_{nitrile}$ [-]	x_{amide} [-]	x_{acid} [-]	Batch time [h]
1	0.15	0.85	-	5
2	0.20	0.80	-	5
3	0.25	0.75	-	5
4	0.90	0.10	-	5
5	0.95	0.05	-	5
6	1	0	-	5
7	0.15	0.85	-	10
8	1	0	-	10
9	0.95	-	0.05	5

Volume batch

The volume of each batch experiment was needed for later. This was calculated by

$$V = \frac{1}{4}\pi d_i^2 L \tag{3.1}$$

where V is the volume in mm^3, d_i the inner diameter in mm and L the length in mm. The obtained volume was converted to mL. The total volume of the batch was calculated volume by adding 2 times the volume of the caps ($V_{cap} = 0.1$ mL). Table 7 shows the actual volume of the reactors.

Autoclave preparation

A stainless steel metal tube was cut into pieces of 60 mm with an internal diameter of 10.35 mm. The inner circle edges and the cylindrical edges were smoothened with an electric drill and a small sanding machine, respectively. Moreover, caps (Swagelok) were placed on both sides of the tubes and were tightened hard to prevent leakages during the experiments. The tops were tightened approximately 5/4 turns in circles - in some cases the tops needed to tighten more. The autoclaves could only be used for a few experiments, then new ones were needed.

Experimental setup

The prepared autoclaves filled with reactants were placed in a metal holder on top of a heater (RKA RH digital). A thermometer was used to determine the temperature during the experiments which was placed in an extra autoclave that was placed on the metal holder with thermo-oil (Ultra 300). This autoclave was covered with aluminum foil so possible gases could not be released and to prevent heat losses at the top of the autoclaves. Afterward, the whole setup was covered. Figure 13 shows the setup of the experiments and the used autoclaves. The experiments were operated at 300 °C (heater set to 310-315 °C) and 300 revolutions per minute (RPM).
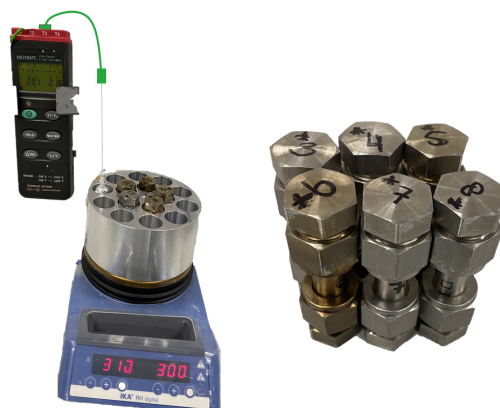
Figure 13: The experimental setup and the prepared mini-autoclaves.

3.1.2 Viscosity experiments

Viscosities of oleic acid, amide and nitrile were measured with the DV2T Viscometer (AMETEK Brookfield) with spindle number 62 and a spindle speed of 100 RPM. Despite the spindle, a magnetic cylindrical stirrer with a length of 50 mm was also used at 100 RPM so that the temperature would remain the same at every point. A glass beaker of 1 L was filled with 800 mL of desired components. Moreover, a heater was used to heat the oleic components and measure the viscosities from 25 to 150 °C, the amide was measured from 80 °C when it was at the liquid phase. The used setup and obtained results are shown in Figure 38 in Appendix A.II.

3.1.3 Vapor-Liquid Equilibrium experiments

Vapor-liquid equilibrium experiments were done with acid/water and nitrile/water, to describe the distribution of these components between the vapor- and liquid phases. The set-up and obtained observations are shown in Appendix A.III.

3.1.4 NMR analysis

Before measuring samples with the NMR, the samples were prepared that contains the following: 0.02 g of an internal standard 1,3,5-Trimethoxybenzene (Sigma-Aldrich), 0.03 - 0.06 g of the desired sample from the experiments and 1 mL of the NMR solvent. The NMR solvent was prepared by mixing 6 mL of Chloroform-d (99.8 atom % D, Sigma-Aldrich), 4.5 mL of Dimethyl sulfoxide-d_6 (99.9 atom % D, Sigma-Aldrich) and 60 μL of Trifluoroacetic acid (VWR) together. After making the samples, this was perfectly mixed with the IKA Vortex 2. Finally, the samples were added into 5 mm diameter NMR tubes using a capillary glass pipette. The volume in the NMR tube should be at least three fingers wide. Moreover, a Bruker Ultrashield 400 MHz NMR spectrometer was used to measure the samples and Mestrenova (14.2.1) for analyzing the obtained data acquired from the NMR spectrometer.

3.2 Simulation

The fatty acid nitrilation was modeled in Aspen Plus (V11) using the property method Non-Random Two Liquid (NRTL). The components oleic acid, ammonia, oleamide, water

and oleonitrile were added to the physical properties. Furthermore, dipole moments were implemented for oleamide (4.04 debye) and oleonitrile (4.58 debye). [30,31]

The forward and backward reactions of the nitrilation process were applied separately as KINETIC reactions. The reaction type POWERLAW is used for the batch reactor, CSTR and TBR, and REACT-DIST for the RDC. Second, the corresponding pre-exponential factor and activation energy were implemented based on molarity and the rate was based on reactor volume. Thus, the simulations do not include catalysts. The effect of a catalyst is described by using lower activation energy for reactions with a catalyst.

However, the kinetic constant for the reaction from nitrile to amide was not available. This kinetic constant, k_{-2}, was determined in Matlab using *lsqnonlin* at a temperature range of 200 to 300 °C. For this calculation Equation 2.8 was used, with the $K_{eq,2}$ values from Chila with 5 % and 70 % headspace (Figure 7) and DFT (Figure 19) and k_2 values from Mekki-Berrada et al., Appelman and Verdonk. After calculating the k_{-2}, all data was displayed in an Arrhenius plot where the slope is defined as $-E_a/RT$. Finally, the activation energy was obtained and used in Equation 2.9 to calculate the corresponding pre-exponential factor at 300 °C. All Matlab codes (calculations) can be seen in Appendix A.IV.

3.2.1 Simulation of autoclave experiments

The batch experiments 1 to 6 were simulated in Aspen (see Appendix A.VI) were simulated using the different kinetic rates, equilibrium constants and reversible mechanisms to determine which showed the best agreement with the experimental compositions obtained with the batch experiments 1-6. The reactant amounts were the same as shown in Table 8, and the exactly used masses are presented in Table 7. It was assumed that C_{12} and C_{18} fatty chains behave the same in the nitrilation process, so chain length would not effect the performance during the process. Thus, the batch simulations have been done with C_{18} chains.

The batch was set at a constant temperature of 300 °C for 5 h. The pressure specifications were set to 'calculate reactor pressure', so the used batch volume (see Table 7 of the experiment could be set. Using this data, Aspen calculated the pressure in each batch simulation.

Moreover, Henry's law constants were implemented for ammonia and water in acid, amide and nitrile. This was performed to see if it affected the results. The temperature dependency of the Henry coefficients was calculated at a temperature range of 25 to 350 °C, and coefficients were calculated in Matlab (Appendix A.V) by using *lsqnonlin*

$$ln\, H_{iA} = a_{iA} + \frac{b_{iA}}{T} + c_{iA}\, ln(T) + d_{iA}T + \frac{e_{iA}}{T^2} \tag{3.2}$$

where a, b, c and d are the coefficients for each Henry component.

3.2.2 Simulation of continuous processes

The CSTR was modeled with the RCSTR block with an ingoing and outgoing stream. Parameters such as temperature, pressure and residence time were varied for this reactor type to

obtain the highest yield to nitrile. Second, the TBR was modeled with the RPlug block and varied with the temperature, pressure and length.

The RDC was designed with the RADFRAC block, varied in reflux, temperature and pressure. The condenser was set to partial-vapor-liquid and reboiler as a kettle. The reboiler duty was set to 3000 kJ s^{-1}. To complete this block, column internals were added from the start stage (after the condenser stage) where the acid flows into the RDC to the end stage (before the reboiler stage) where the ammonia flows. The RDC was implemented as a trayed column with sieve trays. Moreover, the temperature of the condenser, tray spacing and diameter of the column were changed to make the RDC more optimal. The gas- and liquid residence times were calculated by dividing the volume per tray by the volume flow per tray. Then, the total gas and liquid residence times were summed. For each reactor type, the valid phases were vapor-liquid. The set-ups for CSTR, TBR, RDC and the developed model in Aspen are shown in the Appendix A.VI.

First, the reaction acid to amide was implemented to obtain the best optimal parameters for each design. Then, the second reaction amide to nitrile was also implemented in the process with these parameters. It was changed based on the yield to nitrile. Moreover, the space-time yield (STY) was determined for each design

$$STY = \frac{F_{RCN} \, t_R}{V_R} \tag{3.3}$$

where F_{RCN} is the outgoing feed of the nitrile in m^3 h^{-1}, t_R is the reaction time of the reactor in h and V_R is the reactor volume in m^3. It determines the amount of nitrile produced during the reaction time normalized for the reactor volume. This helps compare the different reactor types with each other.

3.2.3 Global nitrile production

It was assumed that worldwide nitrile production was equal to worldwide fatty amine production. In 2019 the fatty amine market was USD 2.9 billion with a 6.5 % CAGR.[13] This was calculated for the fatty amine market 2022 by $2.9 \cdot 10^9 \cdot 1.065^3$. The obtained fatty amine market was USD $3.5 \cdot 10^9$. The price of oleonitrile was USD 0.1 per kg.[32] Thus, the produced mole flow of oleonitrile was 4216 mol s^{-1} in 2022. 1 % of the global oleonitrile production is 42.16 mol s^{-1}. Second, it was assumed that the 1 % was equal to the mole flow of oleic acid in the simulations so there is 100 % conversion. This acid mole flow was used in the simulation of every reactor type.

4 Results and discussion

4.1 Data assessment

In this subchapter, it is shown that experiments had been conducted to evaluate the quality of the kinetics available in the literature, as there are different values and different mechanisms proposed.

4.1.1 The reversibility and equilibrium of amide dehydration to nitrile

There is no clear answer from the literature on the reversibility of the reaction amide to nitrile. But it is still important, because due to the water produced - the reaction can go back from nitrile and water to an amide. When there is no reversibility, the reaction goes only forward to the nitrile side (Equation 4.1) - this is beneficial. On the contrary, if there is reversibility (Equation 4.2) - the nitrilation process can be intensified by the proposed designs for water removal. By removing water from the process, the reaction equilibrium moves towards the nitrile side. This was discussed in Chapter 2.2.2.

$$RCONH_2 \rightarrow RCN + H_2O \tag{4.1}$$

$$RCONH_2 \rightleftharpoons RCN + H_2O \tag{4.2}$$
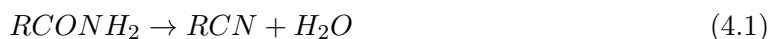
4.1.2 Autoclave experiments

Figures 14a and 14b demonstrate the compositions of the batch experiments before and after 5 h of cycle time. From this data, it can be seen that the compositions are all the same after the 5 h experiment. This does not apply to experiment 6, because here little acid and amide were formed. What is interesting in this data is that experiment 6 contained only nitrile and water in the batch. To be sure that the Lauronitrile used was pure, this was analyzed with the NMR as well. The data obtained showed that the purity of nitrile was 99.6 %, and it contained only 0.4 % acid. The mean composition of experiments 1 to 5 is 12.0 % acid, 50.2 % amide and 37.8 % nitrile. Furthermore, experiments 4 and 5 clearly show that the reaction amide ↔ nitrile is reversible: The reaction started with mole fraction of 0.895 and 0.951 nitrile. Nitrile reverted to amide and acid until the equilibrium composition of a mole fraction of 0.38 nitrile was reached. This fits with the hydrolysis of nitriles to amides described in the literature (see Chapter 2.2.2).[17] The amide ↔ nitrile reaction is therefore considered reversible during the process simulations.
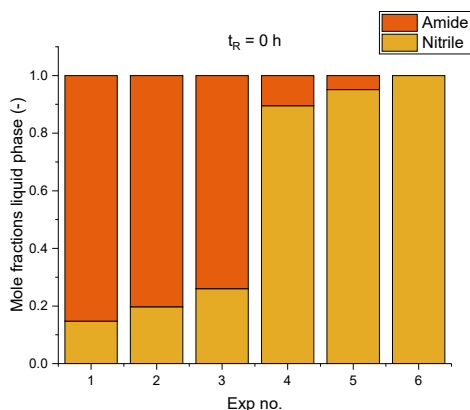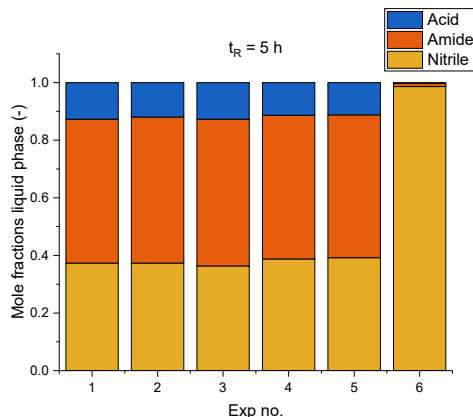
(a) Mole fractions at $t_R = 0$ h.   (b) Mole fractions at $t_R = 5$ h.

Figure 14: Mole compositions in the liquid phase of acid, amide and nitrile of experiments 1-6 at $t_R = 0$ and 5 h; Experiments 1-5 obtained approximately the same equilibrium compositions of acid, amide and nitrile at $t_R = 5$ h.

Experiments with the starting compositions of experiments 1 and 6 were repeated with a reaction time of 10h instead of 5h, to see if there are differences. Figure 15a shows the compositions before the experiments and figure 15b shows the obtained compositions after the experiments. Data from Figure 15b can be compared with the data of experiment 6 in Figure 14b which shows that there is formed more acid and amide after a cycle time of 10 h. Experiments 7 and 8 contain approximately the same molar compositions. The mean composition of these experiments is 11.9 % acid, 49.1 % amide and 39.0 % nitrile. Which is the same equilibrium composition obtained from experiments 1-6. This indicates that the reaction starting from pure nitrile and water takes longer to reach the equilibrium composition than those where amide is present from the beginning.

(a) Mole fractions at $t_R = 0$ h.   (b) Mole fractions at $t_R = 10$ h.

Figure 15: Mole compositions in the liquid phase of acid, amide and nitrile of experiments 7-8 at $t_R = 0$ and 10 h; Experiments 7-8 obtained approximately the same equilibrium compositions of acid, amide and nitrile at $t_R = 10$ h, as compared to Figure 14b.
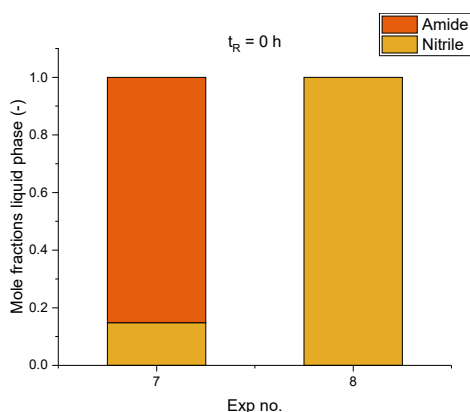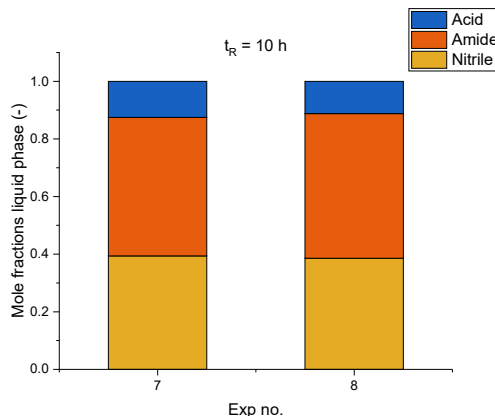
Next, completely different starting compositions were used with acid, nitrile and water in experiment 9. This experiment does not contain amide. Interestingly, for this composition and a cycle time of 5 h, more acid and amide have been formed than in experiment 6. This can be seen in Figure 16. The obtained composition for experiment 9 is 13.9 % acid, 48.7 % amide and 37.4 % nitrile, the same equilibrium composition as obtained with the other experiments. The addition of a small percentage of acid to nitrile sped up the hydrolysis of nitrile to amides so that the equilibrium was reached in 5 h instead of 10. This is explained by the mechanism of nitrile hydrolysis, which is acid catalyzed - in this case, lauric acid acts as the acid catalyst. This also occurs in the other experiments as soon as amide has reverted to acid.
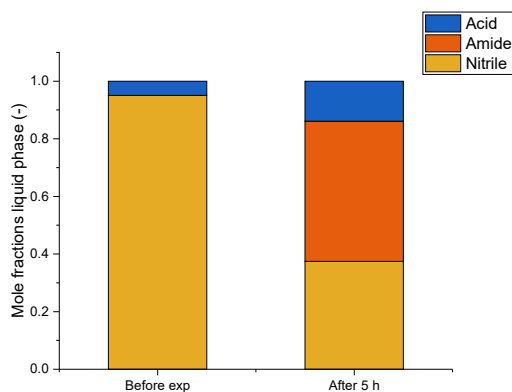
Figure 16: Mole compositions in the liquid phase of acid, amide and nitrile of experiments at $t_R = 0$ and 5 h; At $t_R = 5$ h, approximately the same equilibrium compositions of acid, amide and nitrile are obtained, as compared to Figures 14b and 15b.

Overall, the obtained mean compositions are approximately equal after the experiments. Thus, there is reversibility in the reaction of amide to nitrile and the equilibrium lies on the amide production side and nitrile side.

4.1.3 Simulation of autoclave experiments in Aspen as batch-reactor

In this section, Aspen was used with the different available data for kinetics and the equilibrium constants to simulate the autoclave experiments. They are then compared to the experimental results to determine which combination of kinetic data and equilibrium data can describe the experimental results the best. That set is consequently used to simulate the conventional and intensified nitrilation processes. Table 9 shows the simulation numbers 1, 2, 3 and 4 with the used kinetic data for the simulations. The backward kinetic constant, k_{-2}, is different for these kinetics. Because they were determined with different $K_{eq,2}$ values from Chila with 5 or 70 % headspace and from DFT.

Table 9: Simulation numbers providing the different kinetic data used for the simulations.[4,6,7]

Simulation no.	Kinetic data
1	Mekki-Berrada et al.
2	Appelman
3	Verdonk uncatalyzed
4	Verdonk catalyzed

In the following reasoning (and figures), the terms 'with Henry's law' or 'without Henry's law' are used, where with Henry's law means that the Henry constants were calculated from COSMO-RS and without Henry's law the Henry coefficients were estimated by Aspen.[9]

Figures 17 and 18 show the pressures of the outgoing batch products with batch volumes shown in Table 7. Different equilibrium constants were used from Chila with 5 and 70 % headspaces and DFT, by using kinetic data shown in Table 9. From Figure 17, it can be seen that the pressures of experiments 1-3 are lower than experiments 4-6 by simulating the batch without Henry's law components. One reason for this, is the batch reactors have different starting compositions (Table 7). It can be seen that in experiments 1-3 the mass amount of amide is higher than in experiments 4-6. On the other hand, there is more nitrile and water used in experiments 4-6 than in experiments 1-3. Moreover, Figures 17a and 17c have approximately the same pressure range over the simulation numbers. From these figures, it can also be observed that there are differences in pressure between the simulation numbers 2-4 compared to 1. On the contrary, Figure 17b shows not a lot of difference in the behavior of the used kinetic data from Table 9.

One unanticipated finding in Figure 18 was that adding Henry's law components caused unrealistically lower pressures of approximately 0.1 bar. This is not realistic because a pressure of around 60 bar had been obtained during pressure experiments (see Appendix A.VII). The pressure experiments were with a different headspace and a different starting composition than experiments 1-6. Nevertheless, it gives an estimation in the same range of magnitude for where the pressure is to be as expected. Lower pressures were anticipated since the experiments were processed with higher headspaces. But it was not expected to be only 0.1 bar. Moreover, Figures 18a and 18c show that the pressures of experiments 4-6 are lower than experiments 1-3. This is the opposite of Figures 17a and 17c. Thus, the batches simulated with DFT, Chila 5 % and 70 % headspaces with pressures that behave more as expected.
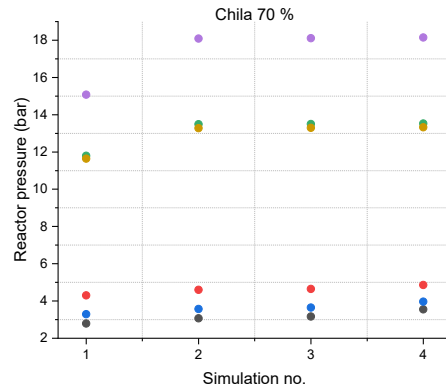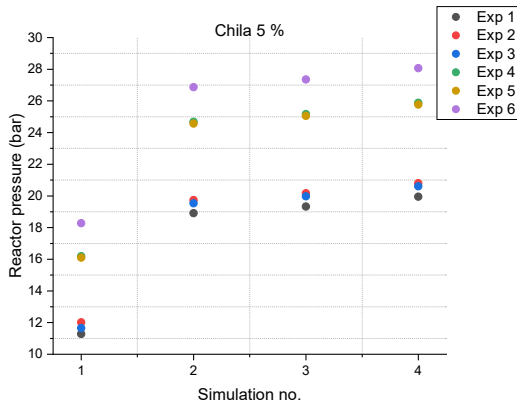
(a) Using $K_{eq,2}$ from Chila 5 %; Pressure over simulation number.

(b) Using $K_{eq,2}$ from Chila 70 %; Pressure over simulation number.
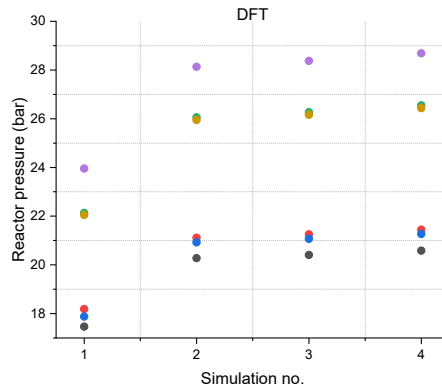
(c) Using $K_{eq,2}$ from DFT; Pressure over simulation number.

Figure 17: Different equilibrium constants ($K_{eq,2}$) were used from kinetic data of Chila 5 and 70 % and DFT; Pressures over different simulation numbers 1, 2, 3 and 4, see Table 9.

27
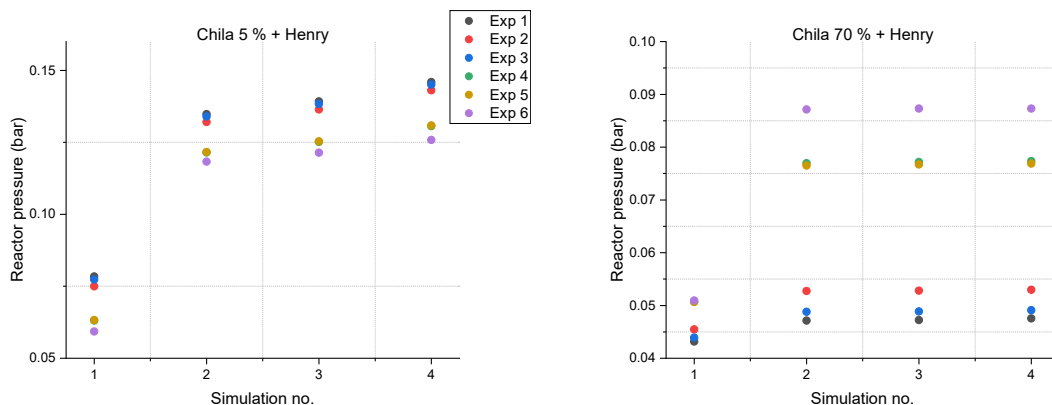
(a) Using $K_{eq,2}$ from Chila 5 %; Pressure over simulation no.

(b) Using $K_{eq,2}$ from Chila 70 %; Pressure over simulation no.
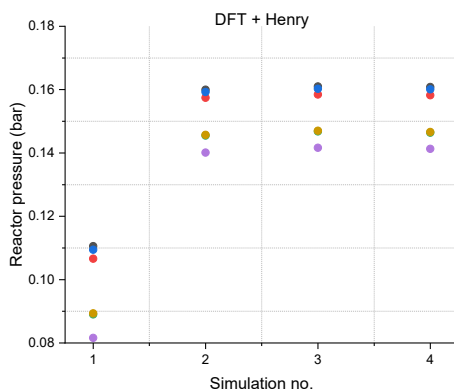
(c) Using $K_{eq,2}$ from DFT; Pressure over simulation no.

Figure 18: Different equilibrium constants ($K_{eq,2}$) were used from kinetic data of Chila 5 and 70 % and DFT; Henry components obtained from Figures 12a and 12b were implemented in the simulation; Pressures over different simulation no. 1, 2, 3 and 4, see Table 9. It can be seen that the pressures are far lower than in Figure 17 - the difference is implementing the Henry components.

Results obtained with equilibrium data from density-functional theory are shown in Figure 19. The subfigures are experiments 1-6, which were simulated with the kinetic data from Table 9. The 'before' compositions are from the experimental data and the simulation data, followed by the obtained mole compositions of the simulations and the experiments. From Figure 19, it is obtained that there is little to no amide shown in simulations 2 to 4 which means that these are not fitting with the experimental data. That leaves only simulation 1. Comparing the experimental data, it can be seen that the compositions correspond relatively well to each other. Figures 19a, 19b, 19c, 19d and 19e show that the compositions correspond relatively well from simulation 1 and the experimental data - only the amide formation is fewer, except in Figure 19f where the experimental data does not contain a lot amide and acid.

This fitting of the DFT data and simulation 1 is also the case when Henry components are added to the process, see Figure 52 (Appendix A.VIII) more amide is formed in simulations 2 to 4. Although, adding Henry components caused low pressures in the process. Thus, this could not be used as the most fitting kinetic data.
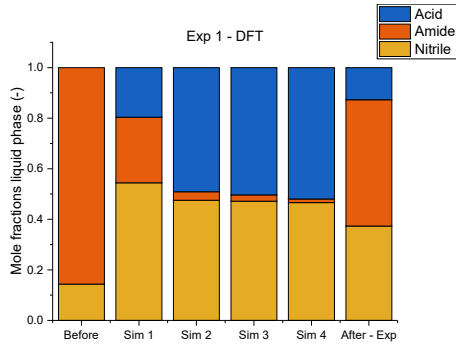
(a) Experiment 1.
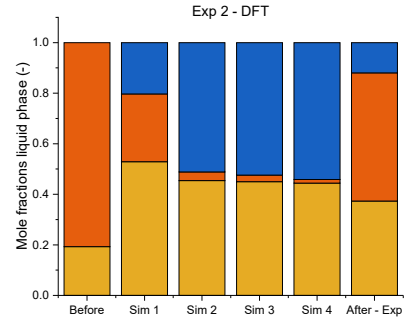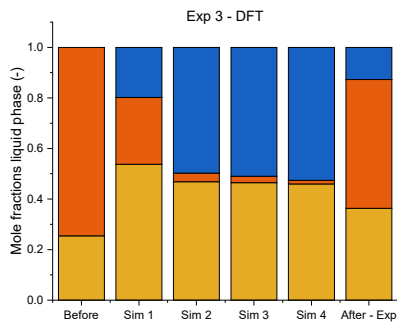
(b) Experiment 2.
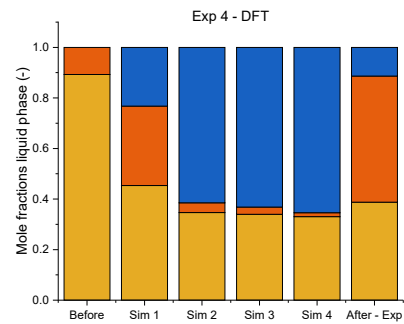
(c) Experiment 3.
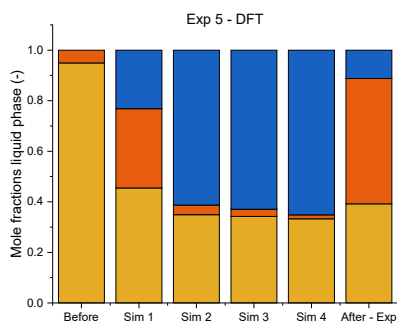
(d) Experiment 4.
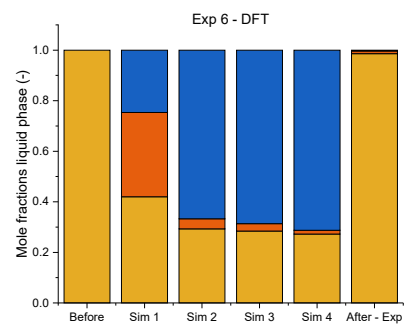
(e) Experiment 5.

(f) Experiment 6.

Figure 19: Mole compositions in the liquid phase of acid, amide and nitrile of experiments 1-6; From left to right: mole compositions before experiment and simulation, simulation 1, 2, 3 and 4 followed by the experimental result at $t_R = 5$ h; Simulations 1-4 used DFT equilibrium data. [9]

Further combinations of kinetic data with different measured equilibrium constants are simulated in Appendix A.VIII. They all show a worse representation of the experimental results and were therefore included only in the appendix to provide a complete picture.

Overall, these results indicate that the most promising and fitting kinetic data the equilibrium constant calculated from DFT-data by using simulation 1 - Mekki-Berrada et al. The next Chapter 4.3, therefore, moves on to simulations using the kinetic data of Mekki-Berrada et al. and DFT.

Now that DFT matched the best, the simulation of the autoclave experiments with this data set can be explored in more detail. The outgoing batch products were containing components in liquid and vapor phases. Figure 20 shows the mole fractions in the vapor phase of ammonia and water obtained in the product streams in experiments 1-6 over time. It can be observed that the ammonia formation starts from a time of 0 to 5 h, where the mole composition ($\approx$0.366) stays at a steady state and reached equilibrium after 3 h. This applies to all experiments 1-6. Water starts at different compositions, this is also shown in Table 7. After 5 h, water is steady-state for all experiments, so it reached a mole fraction of 0.626.
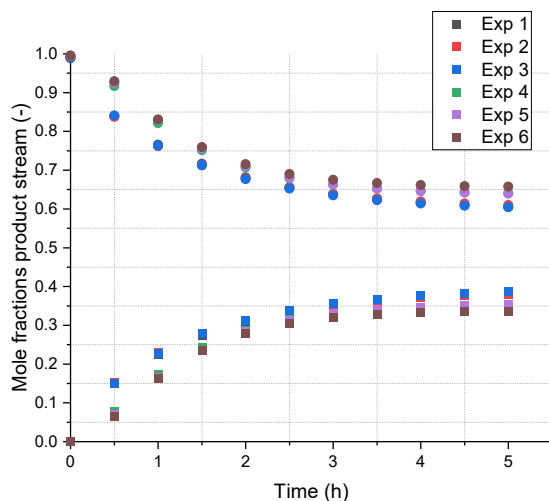
Figure 20: Mole compositions in the vapor phase of ammonia and water over time. The different colors show experiments 1-6. The symbol ● shows the ammonia and ■ the water.

The vapor phase of the batches were containing ammonia and water - the mole compositions are shown in Figure 21. Thus, there was more water ($\approx$ 60 %) in vapor phase than the ammonia ($\approx$ 40 %).
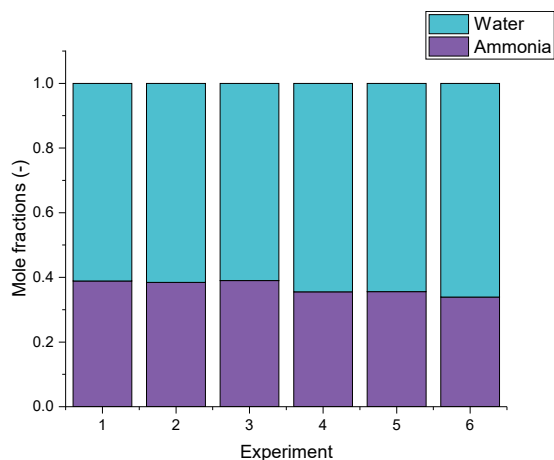
Figure 21: Mole compositions in the vapor phase from the product streams of experiments 1-6, were containing approximately 40 % ammonia and 60 % water.

The pressures of the batch reactors were between 18 and 24 bar (Figure 17c), to see it in more detail the pressures are shown in Figure 22 from start till the end of the batch cycle time. From this graph, it can be seen that the pressures are in a steady state after 3 h. Regardless of whether it starts at a higher or lower pressure, it ends at roughly between 18 and 24 bar. The experiments contain different starting compositions of water (Table 7), so the pressures are higher at experiments 4-6 because there is more water in the vapor phase in the batch reactor. Thus, the operating pressures are lower when the starting water compositions are lower in experiments 1-3. Moreover, it increases because of more formation of water in the process.
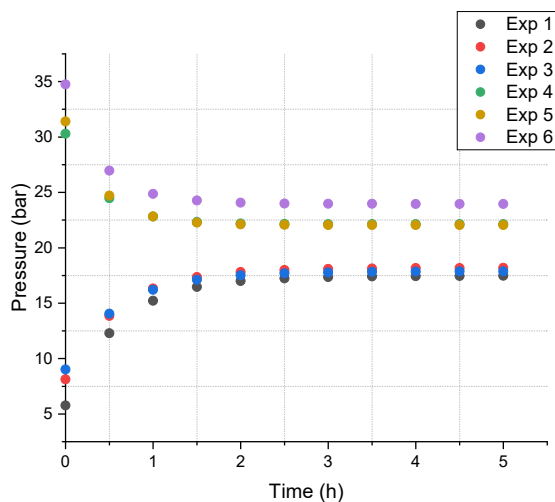
Figure 22: Pressures over time of experiments 1-6; the pressures are in a steady state after 3 h.

Figure 23 shows the outgoing moles of acid, amide and nitrile from experiments 1 and 6 over time. The reactions slow over time in both experiments, so an equilibrium is approached. This

is not confirmed by experimental findings: the composition of acid, amide and nitrile was found to be the same at 5 h and 10 h of reaction, as seen in Figures 14b and 15b.

(a) Experiment 1.   (b) Experiment 6.
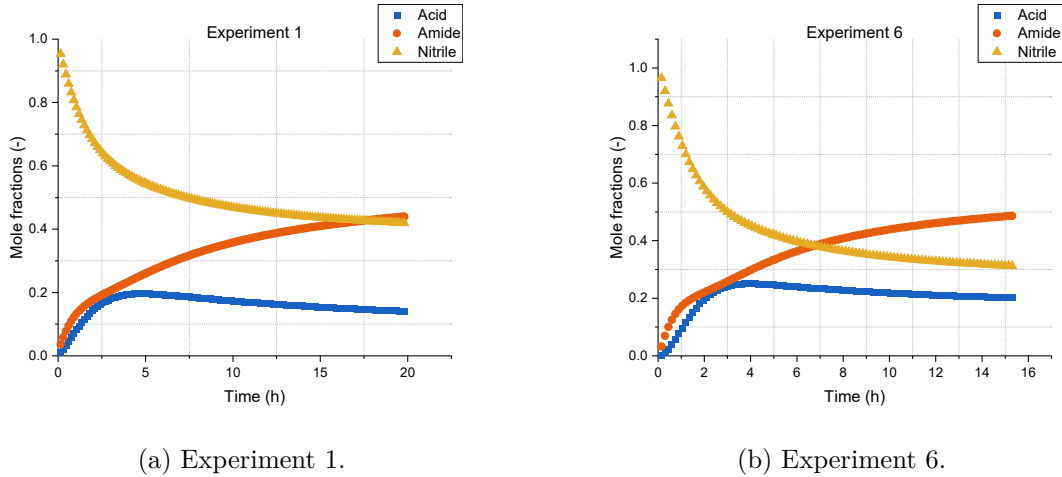
Figure 23: Mole compositions in the liquid phase of acid, amide and nitrile of experiments 1 and 6 over time.

To compare the obtained mole amounts after 10 h with experiments 7 and 8, experiments 1 and 6 were simulated with a cycle time of 10 h. These experiments are shown in Figure 24, where it shows the compositions before (B) and after (A) the experiments. The acid and nitrile formation is more than the amide in experiment 1. Moreover, the mole compositions of experiment 6 show that more acid is formed in the process. All in all, the outcome mole compositions of experiments 1 and 6 correspond relatively well to experiments 7 and 8. Thus, the mole compositions in experiments 1 and 6 with a cycle time of 5 h (Figure 14b) are the same as the compositions obtained with a cycle time of 10 h (Figure 24).
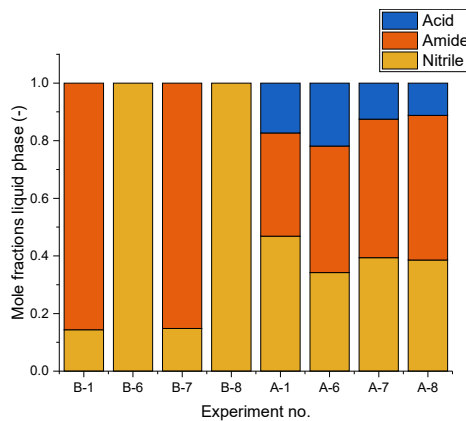
Figure 24: Mole compositions in the liquid phase of acid, amide and nitrile of experiments after 10 h; From left to right: mole compositions of before experiments 1, 6, 7 and 8, followed by compositions of experiments 1, 6, 7 and 8 after 5 h.

4.2 Mathematical evaluation

In the previous section, it is shown that the second reaction amide to nitrile is an equilibrium reaction like the first reaction from acid to amide. When more than one reaction of a reaction system is an equilibrium reaction, the relation between the equilibrium constants is important.

Figure 1 shows the fatty acid nitrilation reaction scheme, so the overall reaction from acid to nitrile is shown below.

$$RCOOH + NH_3 \rightleftharpoons RCN + 2\,H_2O \tag{4.3}$$
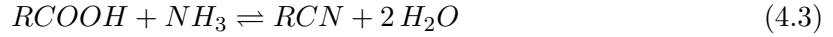
This gives the following relation of the equilibrium constants of the overall reaction

$$K_{eq,acid \to nitrile} = \frac{[RCN][H_2O]^2}{[RCOOH][NH_3]} = \frac{K_{eq,1}}{K_{eq,2}} \tag{4.4}$$

where the $K_{eq,1}$ and $K_{eq,2}$ are defined in Equations 2.7 and 2.8.

From Equation 4.4, it can be seen that the water concentration is squared. This means, that there is more water formation in the overall nitrilation process and that the concentration of the water has a stronger effect on where the equilibrium lies than all other compounds in the mixture. Thus, process intensification in the fatty acid nitrilation is needed to remove the water formed, so that the reaction equilibrium moves toward the nitrile side. Moreover, the amide concentration is removed, so all amide is converted to nitrile or reverted to the acid.

By using process-intensified reactors, the water can be removed during the nitrilation process. For example, if $K_{eq,acid \to nitrile}$ is constant, just as the starting composition of the acid and ammonia fed to the reactor, and the formed water concentration is halved by in situ water removal, the effect on Equation 4.4 will be:

$$[H_2O]^2 = [\frac{1}{2}]^2 = \frac{1}{4} \tag{4.5}$$

where $\frac{1}{4}$ of the water formation remains. Thus, that means more nitrile can be formed. Table 10 shows the obtained equilibrium constants from the best-fitted data as shown in Section 4.1. The equilibrium constant of reaction acid to amide is 8.06, this means that the products are more stable than the reactants. That is the opposite of the equilibrium constant of reaction amide to nitrile because the value is lower than 1. Thus, the reactants are more stable.

Table 10: Equilibrium constants $K_{eq,1}$ determined by using kinetic data of Mekki-Berrada et al. and $K_{eq,2}$ determined by using kinetic data from Mekki-Berrada et al. with DFT equilibrium data. [4,9]

$K_{eq,1}$ [-]	8.06
$K_{eq,2}$ [-]	0.85

4.3 Design

In this subchapter, the most appropriate reactor is chosen and further optimized for the fatty acid nitrilation process, to obtain pure nitrile.

4.3.1 Process development for intensified nitrilation

The fatty amine market is projected to grow until 2024. For this, it is important to further develop the nitrilation process as well. Through the energy-efficient operation, using little ammonia excess and removing water from the process, the nitrilation process can be intensified by different reactor designs such as the CSTR, TBR and RDC. These are carried out by using kinetic data from Mekki-Berrada et al. and DFT as discussed in section 4.1.

The previous subchapter 4.1 showed that the second reaction of amide to nitrile is reversible. Thus, it is important to remove water from the process to shift the reaction equilibrium towards the nitrile side. The goal of this subchapter was to demonstrate which reactor produces the most nitrile with no recycling and no excess of ammonia. The designed reactors are shown in Appendix A.VI with ingoing streams of acid and ammonia containing each 42.2 mol s^{-1}.

CSTR configuration

First, the CSTR is modeled with the reaction of acid to amide varied in temperature at standard conditions of 3 bar and for 5 h. The temperature with the highest yield to amide is used to vary with pressure for 5 h. At last, the pressure with the highest yield to amide is used to vary the residence time. Figure 25 shows the obtained results after varying in three parameters. From Figure 25, it can be seen that by increasing the temperature, the pressure and the residence time - the conversion of acid and yield to amide increases. The most optimal parameters for the initial reaction are the temperature at 300 °C, the pressure at 10 bar and the residence time at 12 h. These parameters give 44 % conversion of acid and 44 % yield to an amide.
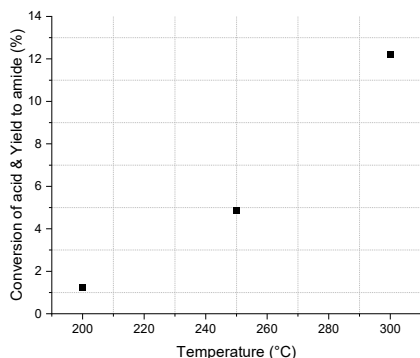
(a) Variation of temperature.
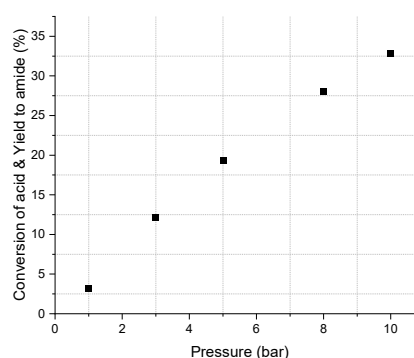
(b) Variation of pressure.
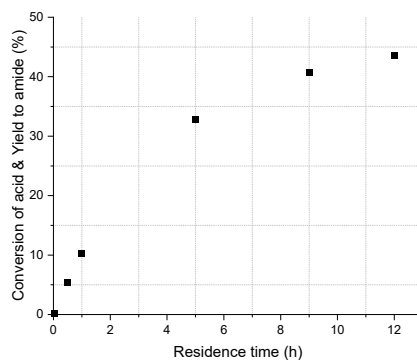
(c) Variation of residence time

Figure 25: Obtained conversion of acid and yield to amide in % from the product stream of the CSTR (Figure 42) over different parameters. The most optimal parameters for the initial reaction are the temperature at 300 °C, the pressure at 10 bar and the residence time at 12 h.

Moreover, both reactions were carried out in the CSTR using the parameters obtained from reaction 1. The highest yield to nitrile is obtained after 12 h, shown in Figure 26 with 46 % conversion of acid, 11 % yield to amide and 35 % yield to nitrile. However, the yield to nitrile is not high enough. In addition, the reactor volume is 11,930 m^3 at this data, which is a large reactor. But there is also a very large product stream obtained, so that is not too unexpected. The space-time yield to nitrile of the CSTR is 31 %, which means that the use of a high volume and time were not efficient enough to obtain high nitrile production. Moreover, the conversions in the CSTR are not high, because there was no in-situ water removal as can be seen in Figure 42, only one product stream. Thus, the presence of water caused, the formed amide reverted to acid in the reactor - so lower conversions were obtained.

Figure 26: Obtained conversion of acid, yield to amide and yield to nitrile in % from the product stream of the CSTR (Figure 42) over different residence time.

Table 11: Optimal parameters obtained for the nitrilation process in CSTR; the best temperature, pressure and residence time for the reaction acid to nitrile and for the overall reaction.

Reaction	Temperature [°C]	Pressure [bar]	Residence time [h]
$RCOOH + NH_3 \rightleftharpoons RCONH_2 + H_2O$	300	10	12
$RCOOH + NH_3 \rightleftharpoons RCN + 2\ H_2O$	300	10	12

Trickle bed reactor configuration

The behavior of reaction 1 is the same in the TBR as in the CSTR, in both reactors, the effect of the catalyst is expressed by using lower activation energy for reactions with the catalyst and no homogeneous or heterogeneous catalysts were used. This can be seen in Figure 27, where the conversion of acid and yield to amide are increased by increasing the temperature, pressure and length. The diameter and length of the TBR were 4 m (for all simulations) and 10 m, respectively, in Figures 27a and 27b. The highest yield to amide is obtained with the temperature at 300 °C, the pressure at 10 bar and a length of 100 m. However, it is not feasible to have a reactor of 100 m. Thus, at a length of 30 m, the conversion of acid and yield to amide are 5 %.

(a) Variation over temperature.
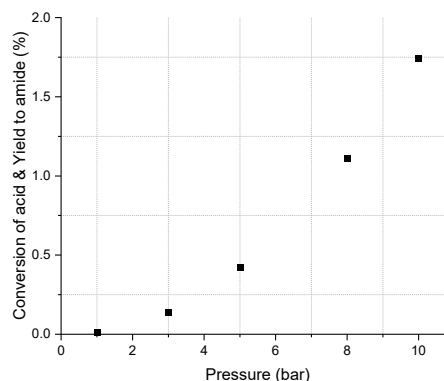
(b) Variation over pressure.
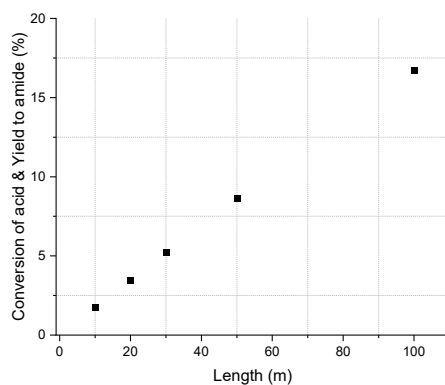
(c) Variation over length.

Figure 27: Obtained conversion of acid and yield to amide in % from the product stream of the TBR (Figure 43) over different parameters.

Figure 28 shows the obtained data including both reactions of the fatty acid nitrilation. At a length of 30 m, the conversion of acid is 5 %, the yield to amide is 4 % and the yield to nitrile is 1 %. These are very low values in a reactor volume of 377 m^3, with also a low STY of 1 %, which means that the use of volume and time were not efficient to obtain nitrile formation. An explanation for this low STY value can be because the residence time is 0.48 h for a 30 m long TBR. This low residence time is not preferred for the reaction amide to nitrile - because it is slow, which means that little nitrile can be formed.
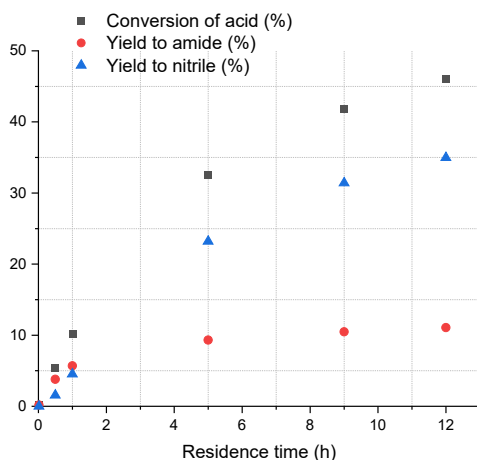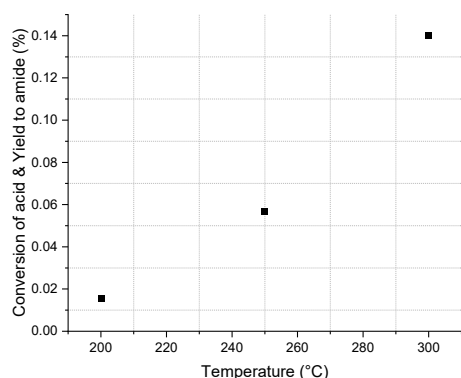
Figure 28: Obtained conversion of acid, yield to amide and yield to nitrile in % from the product stream of the TBR (Figure 43) over different length.

Reactive distillation configuration

The pressure of 10 bar and feed temperature of 300 °C are again the most optimal parameters in the reactive distillation column with sieve trays, see Figures 29b and 29c. On the other hand, a lower reflux ratio of 0.01 gives a higher yield to nitrile, which makes the reactive distillation look more like a stripper. Because the returned liquid back to the column is low compared to the liquid removed as a product from the distillate stream. The conversion of acid and yield to amide are 69 % at these optimal parameters.

(a) Variation over reflux ratio.

(b) Variation over temperature.
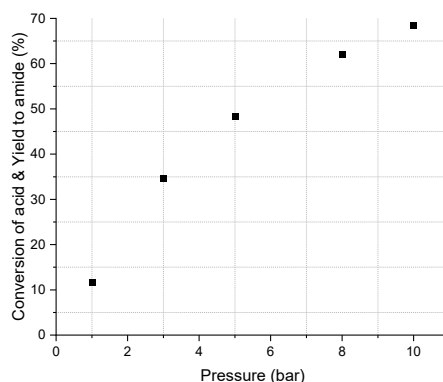
(c) Variation over pressure.

Figure 29: Obtained conversion of acid and yield to amide in % from the product stream of the RDC (Figure 44) over different parameters. Residence times are obtained of Figure 29a at approximately 0.65 h; Figure 29b at approximately 0.7 h; Residence times are increased by increasing pressure: these are between 0.4 - 2.1 h.

By adding the second reaction of amide to nitrile, the conversion of acid, yield to amide and yield to nitrile are 64 %, 26 % and 38 % at 10 bar, respectively. Here, the gas residence time is 0.03 h, faster than the liquid residence time of 0.79 h. What is interesting in Figure 30 is that the yield to nitrile does not rise linearly. But higher yields to nitrile were obtained with the reactive distillation, compared to the CSTR (Figure 26) and TBR (Figure 28) by using in-situ water removal. From the data in Figure 30, it can be seen that the difference in the yield to nitrile between 8 and 10 bar is 0.5 %. However, the conversion of acid is the highest at 10 bar. Moreover, the reactor volume is 28 m^3 and STY is 58 %.
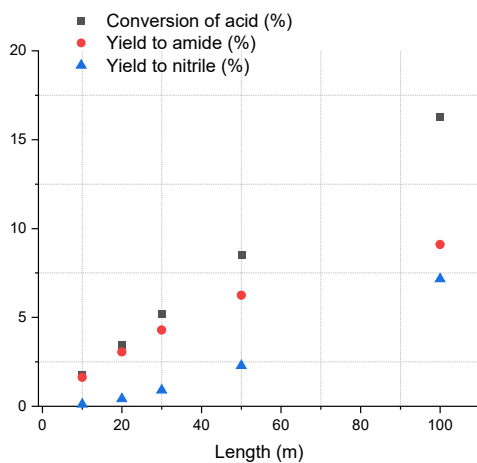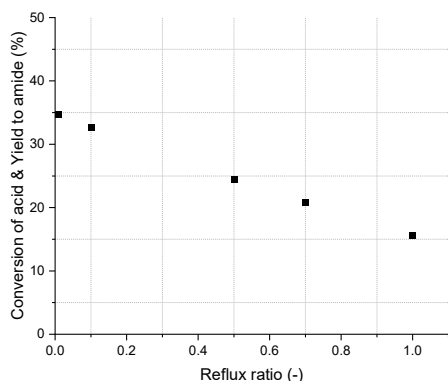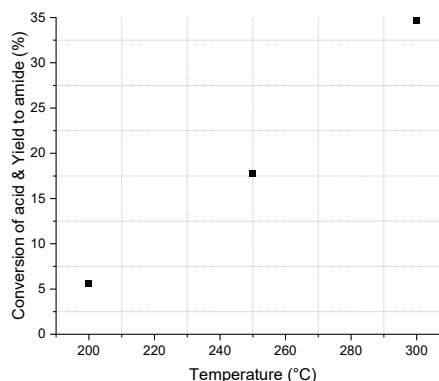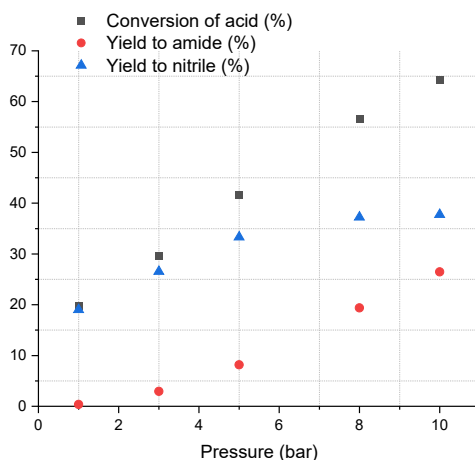
Figure 30: Obtained conversion of acid, yield to amide and yield to nitrile in % from the product stream of the RDC (Figure 44) over different pressures.

In addition, the steady-state column specifications are shown in Table 12. The reactive distillation column had 20 stages, so the reactive zone is from stage 2 to stage 20. This means that the ammonia gas flows into the reboiler stage. The tray spacing is 0.8 m for each stage, so the column has a height of 16 m with 20 stages.

Table 12: Steady-state conditions of the reactive distillation column obtained in Figure 44.

Feed temperature [°C]	300
Acid on stage	2
Ammonia on stage	20
Condenser temperature [°C]	127
Reboiler duty [kJ s^{-1}]	3000
Reflux ratio	0.01
Tray spacing [m]	0.8
Diameter [m]	1.5

The feed temperature is 300 °C, however, this is not constant inside the column. Moreover, the pressure is always constant in the column. The temperature range of the gas and liquid flows are shown in Figure 31. It seems like the temperature from stage 2 to stage 18 decreases to approximately 240 °C, which can have an influence on the reactions. Stage 2 results in a reaction temperature of 300 °C, so the reactions are faster at this stage. Moreover, the reactions slow down when the temperature decreases until stage 28. Figure 29b shows also that higher temperatures ensure higher conversion of acid and yield to an amide. Then, the temperature in Figure 31 is higher at stage 20 because of the reboiler. Interestingly, for these temperature ranges, the acid and nitrile formation is higher than by using a CSTR and a TBR.
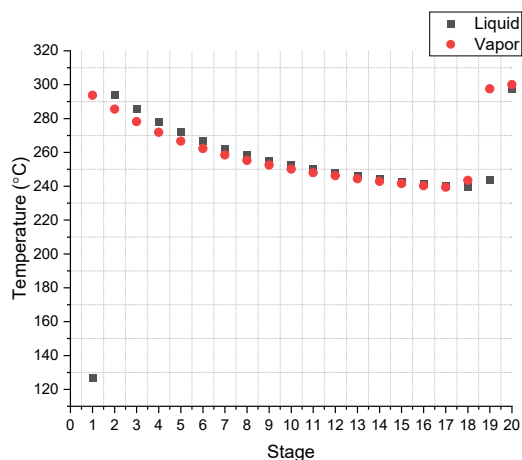
Figure 31: Temperature trend obtained from the RDC in Figure 44; Stage 1 starts at the condenser stage at 127 °C. Then, the acid is fed on stage 2 so the temperatures of the liquid and vapor phase are approximately 300 °C. There is a decrease in liquid temperature from stage 2 to 19 and at stage 20 it is 300 °C again - this is because of the present reboiler. Moreover, the ammonia is fed on stage 20 - therefore the vapor temperature starts at 300 °C - at stage 18 is the temperature lower because of the contact with acid; then the vapor temperature increases from stage 18 to stage 1.

The obtained data with the highest yield to nitrile in the CSTR, the TBR and the RDC are shown in Table 13. All of them gave the highest data at a temperature of 300 °C and a pressure of 10 bar. Because the reaction is faster at 300 °C and there is high ammonia solubility by increasing pressure. It can be seen that the highest conversion of acid is obtained with the RDC in 0.46 h. Moreover, the highest yield to nitrile is obtained with reactive distillation. However, the yield to nitrile in the CSTR does not differ much from the RDC. Only the conversion of acid is lower.

Table 13: Best obtained results of the reactor designs with the residence time in h, conversion of acid and yield to nitrile in %; CSTR, TBR and RDC.

Design	Liquid residence time [h]	Conversion of acid [%]	Yield to nitrile [%]	STY [%]
CSTR	12	46	35	31
TBR	0.48	5	1	1
RDC	0.79	64	38	58

Thus, the RDC demonstrates the best data relative to the nitrile. The residence time of the RDC is low. As mentioned in the Theoretical background in Table 6, the second reaction of amide to nitrile is very slow. So, more residence time is needed. However, more residence time in the RDC means using more stages, which also increases the height of the column. This can only be done to a certain degree. So, using only RDC as a reactor design does not perform the best.

4.3.2 Developed model

The performance of the reactive distillation column designed in the previous chapter can be increased by adding a second reactor. It is more efficient to add the CSTR after the RDC (as a developed model) containing 50 stages so that the acid conversion is the highest in the reactive distillation and also nitrile is formed. After this, more nitrile can be formed in the CSTR with a residence time of 12 h. This proposed developed model design is shown in Figure 32. Another possibility for intensifying the nitrilation process was using two units of reactive distillation columns. However, after research, it was found that this was not optimal for nitrile production.
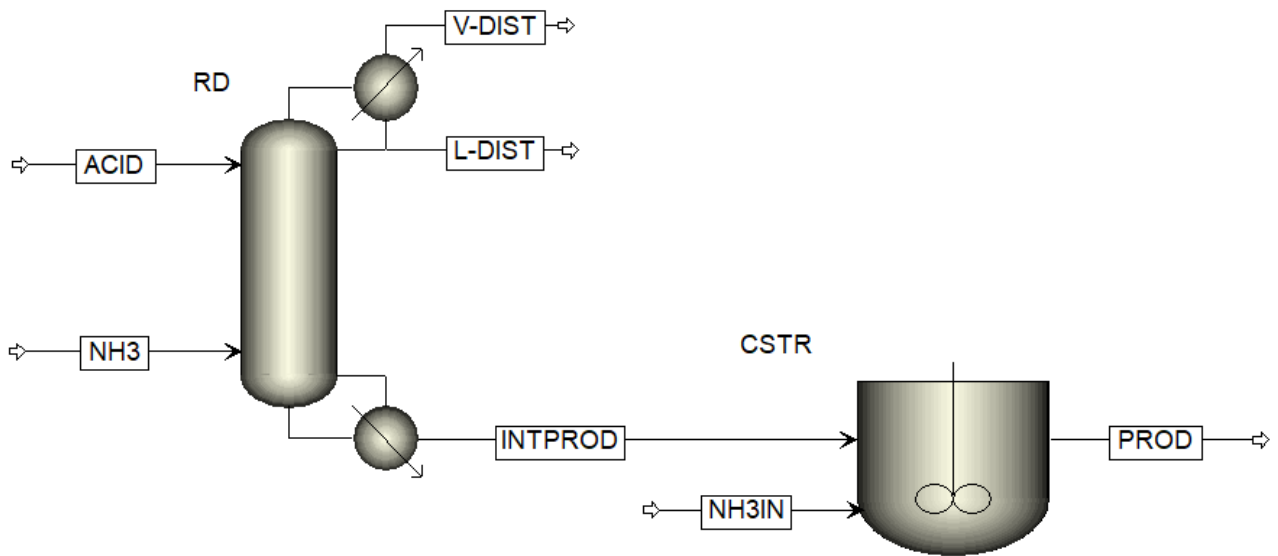
Figure 32: Set-up for the developed model 1 in Aspen.

Both reactions take place in both reactors, so there is an ammonia gas stream added to the CSTR to avoid the back reaction of amide to acid. The feed temperature of the RDC was 300 °C and the volume was 79 m^3, all other steady-state conditions are shown in Table 14. The CSTR was operated at 300 °C and 1 bar over 12 h of residence time. Compared to the optimal parameters obtained in section 4.3.1, the used pressure here was changed to 1 bar due to higher nitrile formation. This reactor had a volume of 71,130 m^3 because very big feed streams were used for the simulations (see section 3.2.3). With this set-up, overall, the developed model 1 has obtained the following results in Table 15. By using two units such as the reactive distillation column and the CSTR, there is an increase in the conversion of acid and yield to nitrile compared to Table 13.

Table 14: Steady-state conditions of the reactive distillation column obtained in Figure 32.

Acid feed on stage	2
Ammonia feed on stage	50
Condenser temperature [°C]	185
Pressure [bar]	10
Reboiler duty [kJ s^{-1}]	3000
Reflux ratio	0.01
Tray spacing [m]	0.5
Diameter [m]	2

Table 15: Obtained results from model 1 shown in Figure 32 using steady-state conditions of Table 14 with a feed temperature of 300 °C. The conversion of acid and yield to nitrile is improved compared to Table 13.

	Model 1
Conversion of acid [%]	73
Yield to amide [%]	4
Yield to nitrile [%]	69
Selectivity to nitrile [%]	94

Figure 33a shows the temperature range over the stages in the RDC, which is the same range as Figure 31. Moreover, the fractions of the components in the product stream (PROD), liquid distillate (L-DIST) stream and vapor distillate (V-DIST) stream are shown in Figure 33b. Almost all ammonia and water are in the vapor phase flowing from the vapor distillate stream. However, there are small amounts of ammonia and water present in the liquid distillate stream and product but these can be easily removed. Moreover, all unreacted fatty acids, side product amide and desired nitrile are in the product stream and only a small amount of acid is present in the liquid distillate stream.
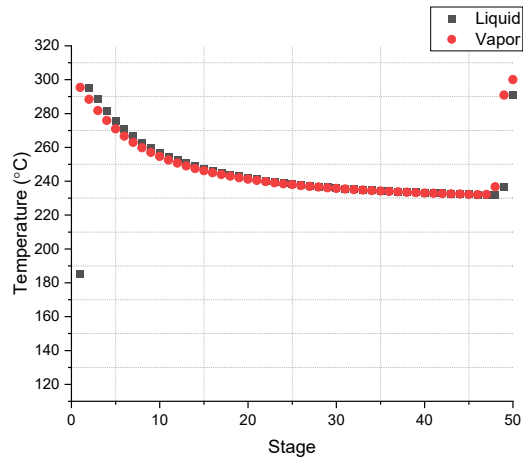
(a) Decrease in liquid temperature from stage 1 to 50 and increase of vapor temperature from stage 50 to 1.
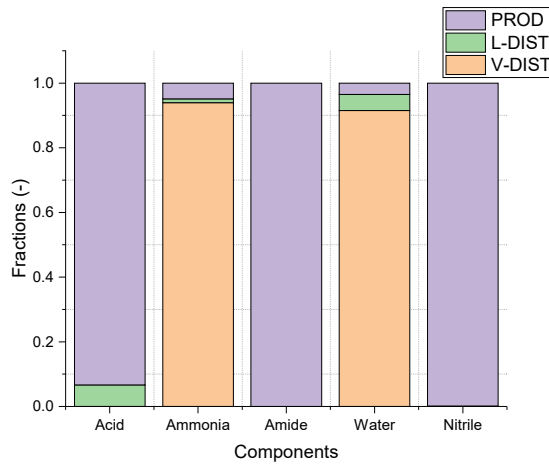
(b) Fractions of the components acid, ammonia, amide, water and nitrile that were present in the product-(PROD), liquid distillate (L-DIST) and vapor streams (V-DIST) of the developed model.

Figure 33: Parameters from the RDC of the developed model 1.

The goal was to intensify the nitrilation process by in-situ water removal and to obtain nitrile as much as possible. Taken together from the previous sections, water can be removed from the top of the column easily with a reactive distillation. Moreover, to produce nitrile the residence time needs to be high enough. Thus, this can be obtained by using the RDC and CSTR together, even without using an ammonia excess in the system. The reactive distillation intensifies the nitrilation process by in-situ water removal, so a high conversion of acid can be obtained. Followed by the CSTR, all obtained amides from the RDC have more residence time in the CSTR to react further to nitrile. Because the reaction amide to nitrile is very slow, this is not suitable for reactive distillation.

4.3.3   Downstream processing

In this section, the developed model 1 has been made more efficient by adding a low NH_3 excess, so more acid reacts to an amide. Furthermore, lower ammonia excess is desired because it is more sustainable. Moreover, the obtained product nitrile and other side products are purified from the vapor distillate, liquid distillate and product streams. A schematic overview of these different models is shown in Table 16, where each time modifications are added to make the developed model more efficient.

Table 16: Schematic overview of used model numbers and the description of added modifications.

Model no.	Description of modifications in the developed model; RD + CSTR
1	No excess of ammonia is added to the system.
2	Excess of ammonia (1:2) is added in both reactors.
3	Purification steps and recycles are added.
4	The CSTR has an outgoing liquid- and vapor stream

First, the developed model 2 in Figure 32 is operated with a 1:2 mole ratio excess of ammonia and with the parameters from Table 14. The excess is added to both reactor designs because they contain the two reactions of the fatty acid nitrilation. The excess of ammonia is supposed to avoid the back reaction of amide to acid. Adding excess resulted in 79 % conversion of acid, 4 % yield to amide, 74 % yield to nitrile and 94 % selectivity to nitrile. Surprisingly, there is only a 6 % increase in the conversion of acid and a 5 % increase in the yield to nitrile related to without adding excess. These differences are shown in Table 17. However, this excess of NH_3 was an advantage for models 3 and 4 because purified acid was recirculated back to the column.

Table 17: *Updated version of Table 15*; Obtained overall results from model 1 and 2 using steady-state conditions of Table 14 with a feed temperature of 300 °C. Results of model 2 shows that there is 6 % increase in the conversion of acid and 5 % increase in the yield to nitrile related to model 2.

	Model 1	Model 2
Conversion of acid [%]	73	79
Yield to amide [%]	4	4
Yield to nitrile [%]	69	74
Selectivity to nitrile [%]	94	94

Next, the liquid distillate, vapor distillate and product streams from Figure 32 are further developed to obtain purified nitrile. This model no. 3 design is shown in Figure 34. Flash drums (F1, F2, F3 and F4) are used to separate the oleic components acid, amide and nitrile from the gasses ammonia and water. Moreover, the nitrile is separated from the acid and amide by using a component separator block. This separation could be designed with a distillation column because it would be easy to separate nitrile from acid and amide - they are no azeotropes. But this separation is out of scope. The focus was on the effect of the recycling containing acid and amide on the process in the next steps.
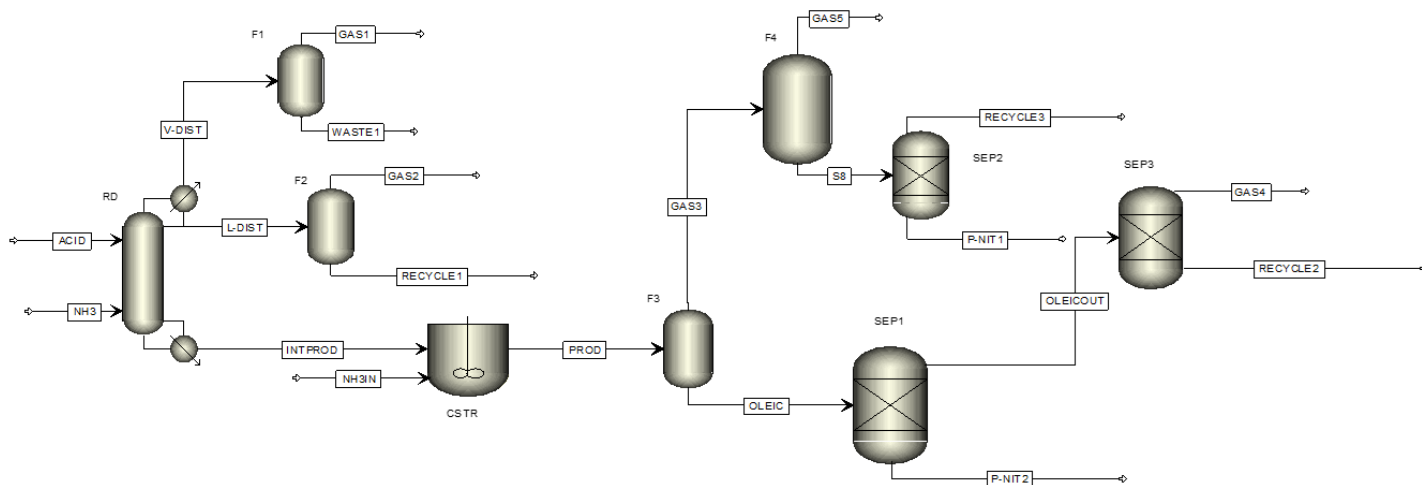
45

Figure 34: Set-up for the developed model 3 in Aspen.

The flash specifications are shown in Table 18, where the pressure and molar vapor fractions were implemented in Aspen. So, the temperature was obtained from the process.

Table 18: Specifications of the flash drums used in Figure 34.

Specifications	F1	F2	F3	F4
Temperature [°C]	84	175	226	190
Pressure [bar]	1	0.1	0.1	0.1
Molar vapor fraction [-]	0.998	0.541	0.130	0.864

Thus, with the use of purification steps - nitrile is obtained in the streams P-NIT1 and P-NIT2. Next, the recycle streams called RECYCLE1, RECYCLE2 and RECYCLE3 have been fed back into the process. Table 19 shows the overall conversion of acid, yield to amide, yield to nitrile and selectivity to nitrile. All the acid was converted, and there was only a 2 % loss in the waste streams. The developed model has improved by adding the recycles to the system.

The last change in the developed model 4 was that the product stream of the CSTR was separated without using flash drum F3. Thus, the CSTR has two outgoing streams the liquid and vapor streams. Overall, model 4 is shown in Figure 53, where the outgoing GAS5 was also separated to obtain more nitrile. The overall conversion of acid, yield to amide, yield to nitrile and selectivity to nitrile are 98 %, 0 %, 98 % and 100 %, respectively.

Table 19: *Updated version of Table 17*; Obtained overall results from models 1-4 using steady-state conditions of Table 14 with a feed temperature of 300 °C.

	Model 1	Model 2	Model 3	Model 4
Conversion of acid [%]	73	79	98	98
Yield to amide [%]	4	4	0	0
Yield to nitrile [%]	69	74	96	98
Selectivity to nitrile [%]	94	94	99	100

Gas streams 1, 2 and 4 were containing ammonia and water in Figure 53. Moreover, ammonia was not removed from the water, so it is not recycled back into the process. When it would be recycled, the process could be improved by 2 percent. On the other hand, it can be more interesting if there are higher prices of ammonia.

Figure 35 shows the temperature range of the liquid and vapor phases over the 50 stages of the developed model 4. The liquid phase starts at stage 1 at 185 °C, this is the condenser temperature. Then, the liquid is at 286 °C because the acid is flowing into stage 2. After that, the temperature of the liquid and vapor are decreasing to 220 °C in the process. Lastly, the temperatures are increasing at stages 49 and 50 because of the present reboiler.
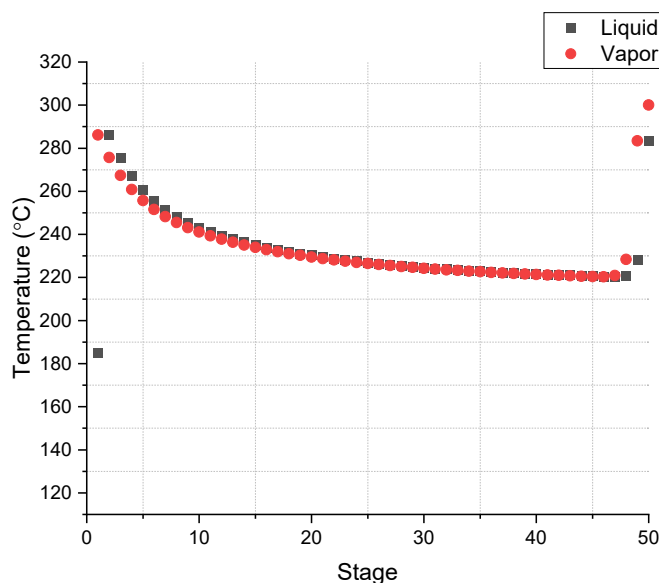

Figure 35: Temperature range from the RDC of the final developed model shown in Figure 53; Liquid temperature from stage 1 to 50 and vapor temperature from stage 50 to 1.

From the final model, it is interesting to note that the fractions of ammonia and water are decreased in the product and liquid distillate streams in Figure 36 compared with Figure 33b. This could be possible because of the use of more stages in the reactive distillation column. Another important effect could be the condenser temperature of 185 °C. Low temperatures have an effect on the reaction rates - as a result, reactions are slower at this stage.
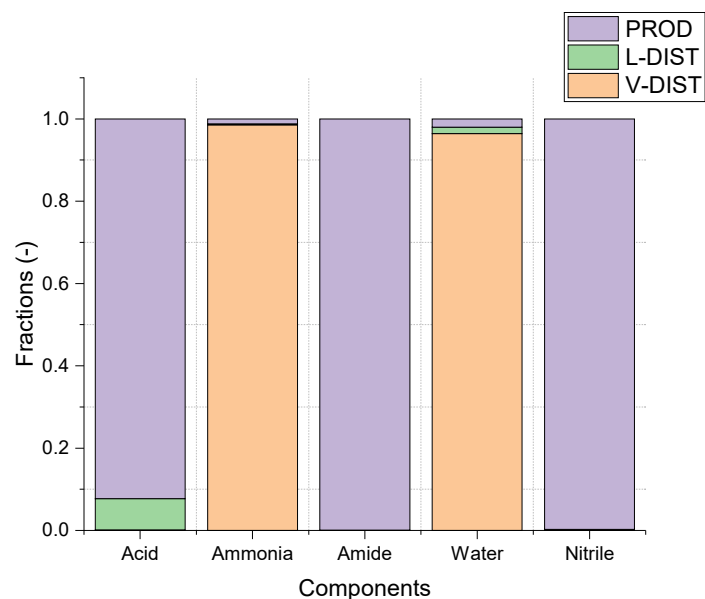
Figure 36: Fractions of the components acid, ammonia, amide, water and nitrile that were present in the product- (PROD), liquid distillate (L-DIST) and vapor streams (V-DIST) from the RDC of the final model.

Overall, the obtained results of the developed model are shown in Figure 37. Model 1 was the process without an excess of ammonia, 2 with a 1:2 mole ratio excess, 3 where the process was purified and recycles were added and 4 the final design by optimizing the outflow of the CSTR. By adding an excess, adding the recycles and purifying the product nitrile, the yield was increased by 29 % (Model 1 vs model 4). Moreover, all amide produced was immediately converted to nitrile. Finally, all acid was converted in the system. Overall, 39,185 kg h^{-1} of pure nitrile is obtained by using the final model in Figure 53.
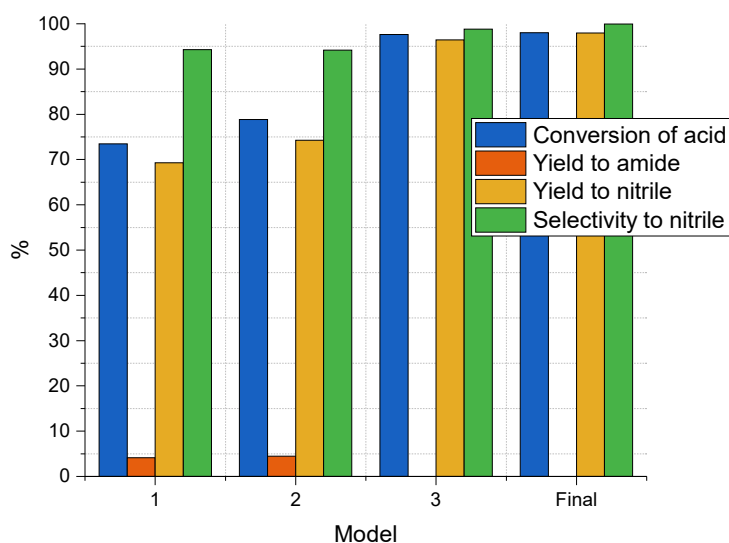
Figure 37: Results of the overall conversion of acid, yield to amide, yield to nitrile and selectivity to nitrile obtained from the different models; 1 = without excess of ammonia, 2 = 1:2 mole ratio of excess added, 3 = process if purified and recycled, 4 = also the CSTR outflow is optimized.

4.3.4 Comparison to semi-batch benchmark

In industry, the semi-batch reactor is used. After operating with different process configurations, the best design was found to be the reactive distillation column followed by the CSTR - that obtained the overall conversion of acid, yield to amide, yield to nitrile and selectivity to nitrile as 98 %, 0 %, 98 % and 100 %, respectively.

The semi-batch benchmark is the data obtained from Mekki-Berrada et al., where an excess of ammonia is used (1.8 times the required stoichiometric value for 6 h) by operating at 300 °C. This caused all acid to be converted after 2 h. Moreover, 98 % yield to nitrile was obtained after 6 h. Interestingly, this yield is also obtained with the developed model.

A drawback of the intensified model is the long reaction time of 12 h in the CSTR, in the semi-batch, which runs for 6 h. But the developed model operates continuously, which the semi-batch reactor does not. This gives the nitrilation production the advantages of continuous operation, namely acid and ammonia were fed continuously, more economic, efficient and high capacity and better product quality.

The main difference between these two models is that the semi-batch benchmark is obtained at a lab scale and the developed model is obtained on an industrial scale in Aspen with the kinetic data from Mekki-Berrada. Moreover, the developed model contains reversible reactions and the semi-batch benchmark assumed that the second reaction of amide to nitrile was only a forward reaction. It was shown that the second reaction is reversible, which needs to be included in the model but that was not done in the kinetic model of Mekki-Berrada et al.[4]

Another better feature of the developed model is that there is used an excess of ammonia, but only 2 times the required stoichiometric value for 12 h. If the semi-batch benchmark would operate for 12 h, the excess of ammonia would be equal to 3.5 times the required stoichiometric value. Thus, the developed model used less excess ammonia which is better because it is more sustainable. Furthermore, if desired, using no ammonia excess at all in the developed model would lead only to a loss of nitrile yield of 2% as shown in section 4.3.3, therefore it is possible to reduce the amount of ammonia even further if the small decrease in yield is acceptable.

5 Conclusion and Outlook

This study set out to determine how fatty acid nitrilation can be intensified using an innovative reactor concept. As a first step, experiments were done to determine the quality of different kinetics available in the literature. From the experimental part, it can be concluded that the reaction from amide to nitrile is reversible. The obtained mean equilibrium composition of experiments 1-5 is 12.0 % acid, 50.2 % amide and 37.8 % nitrile. Thus, the reaction equilibria favor the production of the amide and nitrile sides of the two reactions respectively.

Moreover, batch simulations of the experiments were done to compare the outcome OR results with the experimental results - to determine which kinetic data and equilibrium data can describe the experimental results the best. This research has shown that the best fit was obtained with the equilibrium constant determined from DFT by using kinetic data of Mekki-Berrada et al. These obtained kinetics were used further in the simulation of process-intensified reactors. One finding to emerge from this study is that using Henry coefficients from COSMO-RS were giving unrealistically low pressures in the batch simulations relative to Henry constants that were estimated by Aspen.

The findings of the study of the different process configurations showed that reactive distillation was the best for in-situ water removal. However, only 38 % yield to nitrile was obtained in 0.79 h in the RDC including the two reversible reactions of the fatty acid nitrilation. So, the reactive distillation was not suitable at this reaction time - because more residence time was needed for the slow reaction of amide to nitrile.

Therefore, the optimized design was a reactive distillation column followed by a CSTR, where the RDC was more for the reaction of acid to amide with in-situ water removal and CSTR for high production of nitrile. This developed model resulted in 73 % conversion of acid, 4 % yield to amide, 69 % yield to nitrile and 94 % selectivity to nitrile.

This model was made more efficient by adding a reduced excess of ammonia, purifying the outcome streams and recycling acid and amide back to the model, resulting in an overall 98 % conversion of acid, 0 % yield to amide, 98 % yield to nitrile and 100 %. All acid that was present in the model was converted, so there was a mass loss of 2 %.

Greener chemistry can be achieved by using more renewable fatty acids by processing fatty acid nitrilation. More research is needed to bring this project into reality. This research brought up questions in need of further investigation. It would be interesting to experiment with reactive distillation on a lab scale by using acid and ammonia as continuous streams.

Further research is needed for the separation of ammonia from water, but also the separation of nitrile from acid and amide. This can be done with distillation columns in Aspen. Moreover, research can be done more in-depth about the separations.

Researches of Appelman and Verdonk were done with an alumina catalyst. Thus these studies can be repeated with a new catalyst zinc oxide because Mekki-Berrada et al. obtained a better kinetic model with it.

Lastly, more batch experiments can be done with different starting compositions of acid, amide and nitrile over different times. To determine if the obtained results are fitting well, and to explore the reaction equilibria at different reaction conditions.

References

[1] S. G. Koenig and B. Dillon, "Driving toward greener chemistry in the pharmaceutical industry," *Current Opinion in Green and Sustainable Chemistry*, vol. 7, pp. 56–59, 10 2017.

[2] B. Izzo, C. L. Harrell, and M. T. Klein, "Nitrile Reaction in High-Temperature Water: Kinetics and Mechanism," *AIChE Journal*, vol. 43, no. 8, pp. 2048–2058, 1997.

[3] Y. Shirazi, H. Tafazolian, S. Viamajala, S. Varanasi, Z. Song, and M. J. Heben, "High-Yield Production of Fatty Nitriles by One-Step Vapor-Phase Thermocatalysis of Triglycerides," *ACS Omega*, vol. 2, no. 12, pp. 9013–9020, 2017.

[4] A. Mekki-Berrada, S. Bennici, J. P. Gillet, J. L. Couturier, J. L. Dubois, and A. Auroux, "Ammoniation-dehydration of fatty acids into nitriles: Heterogeneous or homogeneous catalysis?" *ChemSusChem*, vol. 6, no. 8, pp. 1478–1489, 2013.

[5] K. D. Brito, S. F. Vasconcelos, G. F. Neto, A. S. Damasceno, M. F. Figueirêdo, W. B. Ramos, and R. P. Brito, "Semi-batch industrial process of nitriles production: Dynamic simulation and validation," *Computers and Chemical Engineering*, vol. 119, pp. 38–45, 2018.

[6] D. Appelman, *Nitrilation of oleic acid in a gamma-Al2O3 coated microcapillary.* Bachelor thesis, 2021.

[7] L. Verdonk, *Intensification of continuous flow nitrilation in catalyst coated capillaries and packed bed reactors.* Master thesis, 2022.

[8] A. Chila, *Determination of different reaction equilibria as basis for the intensification of fatty acid nitrilation.* Bachelor thesis, 2021.

[9] C. Raffel, "Process intensified production of fatty acid nitriles," Ph.D. dissertation, Eindhoven University of Technology, Manuscript in preparation., 2023.

[10] F. O. Cedeño González, M. M. Prieto González, J. C. Bada Gancedo, and R. Alonso Suárez, "Estudio de la densidad y de la viscosidad de algunos ácidos grasos puros," *Grasas y Aceites*, vol. 50, no. 5, pp. 359–368, 1999.

[11] A. Mekki-Berrada, S. Bennici, J. P. Gillet, J. L. Couturier, J. L. Dubois, and A. Auroux, "Fatty acid methyl esters into nitriles: Acid-base properties for enhanced catalysts," *Journal of Catalysis*, vol. 306, pp. 30–37, 2013. [Online]. Available: http://dx.doi.org/10.1016/j.jcat.2013.05.032

[12] H. Liu, T. Cheng, M. Xian, Y. Cao, F. Fang, and H. Zou, "Fatty acid from the renewable sources: A promising feedstock for the production of biofuels and biobased chemicals," *Biotechnology Advances*, vol. 32, no. 2, pp. 382–389, 2014. [Online]. Available: http://dx.doi.org/10.1016/j.biotechadv.2013.12.003

[13] "Fatty Amines Market Share, Size, Trends - 2019-2024," 2020. [Online]. Available: https://www.marketsandmarkets.com/Market-Reports/amines-market-724.html

[14] F. Bizhanov, "Studying the kinetics of the nitrilation reaction of aliphatic C10-C22 acids," ., 1985.

[15] D. Harvey, *Modern Analytical Chemistry*, 1st ed. The McGraw-Hill Companies, 2000.

[16] P. Atkins, J. de Paula, and J. Keeler, *Pshysical chemistry*, 11th ed. OXFORD University press, 2018.

[17] S. Farmer, "Conversion of nitriles to amides," 2022. [Online]. Available: https://chem.libretexts.org/Bookshelves/Organic_Chemistry/Supplemental_Modules_ (Organic_Chemistry)/Nitriles/Reactivity_of_Nitriles/Conversion_of_nitriles_to_ amides#:~:text=Nitrilescanbeconvertedto,acceptwater%2Capoornucleophile

[18] H. S. Fogler, *Elements of chemical reaction engineering.* Boston: Pearson education, 2016.

[19] P. Trambouze and J. Euzen, *Chemical reactors: from design to operation.* Editions Technip, 2004.

[20] K. Plumb, "Continuous Processing in the Pharmaceutical Industry: Changing the Mind Set," *Chemical Engineering Research and Design*, vol. 83, no. 6, pp. 730–738, 6 2005.

[21] D. Etit, D. E. Eertwegh, and M. F. Neira D'Angelo, "Advanced chemical reactor engineering," in *Draft reader.* ., 2021, pp. 1–142.

[22] A. A. Kiss, M. Jobson, and X. Gao, "Reactive Distillation: Stepping Up to the Next Level of Process Intensification," *Industrial and Engineering Chemistry Research*, vol. 58, no. 15, pp. 5909–5918, 4 2019. [Online]. Available: https://pubs.acs.org/doi/full/10.1021/acs.iecr.8b05450

[23] G. J. Harmsen, "Reactive distillation: The front-runner of industrial process intensification: A full review of commercial applications, research, scale-up, design and operation," *Chemical Engineering and Processing: Process Intensification*, vol. 46, no. 9, pp. 774–780, 9 2007.

[24] R. Khaledi and P. R. Bishnoi, "A method for modeling two- And three-phase reactive distillation columns," *Industrial and Engineering Chemistry Research*, vol. 45, no. 17, pp. 6007–6020, 8 2006. [Online]. Available: https://pubs.acs.org/doi/full/10.1021/ie051384a

[25] M. F. Malone and M. F. Doherty, "Reactive distillation," *Industrial and Engineering Chemistry Research*, vol. 39, no. 11, pp. 3953–3957, 2000.

[26] R. Taylor and R. Krishna, "Modelling reactive distillation," *Chemical Engineering Science*, vol. 55, no. 22, pp. 5183–5229, 2000.

[27] A. B. de Haan and H. Bosch, *Fundamentals of Industrial Separations*, 2nd ed. De Gruyter, 2007.

[28] M. A. A. Alharthi, "Dynamics and Control of Reactive Distillation Process for Monomer Synthesis of Polycarbonate Plants," *Chemical Engineering Journal*, 2014.

[29] M. K. Singh and A. Singh, "Nuclear magnetic resonance spectroscopy," *Characterization of Polymers and Fibres*, pp. 321–339, 2022. [Online]. Available: https://linkinghub.elsevier.com/retrieve/pii/B9780128239865000117

[30] "Oleamide - properties," 2016. [Online]. Available: http://pqr.pitt.edu/mol/FATBGEAMYMYZAF-KTKRTIGZSA-N

[31] "Dipole moment - oleonitrile; COSMO-RS," 2022.

[32] "Guidechem oleonitrile USD prices per kg," 2022. [Online]. Available: https://www.guidechem.com/cas/112-91-4.html

Appendix

A.I   Data of entropy and enthalpy

Table 20: Data of entropy and enthalpy to determine the Gibbs energy.[9]

Reactions	ΔH [kJ mol^{-1}]	ΔS [kJ mol^{-1}]
RCOOH + NH$_3$ $\rightleftharpoons$ RCONH$_2$ + H$_2$O	1.31	0.027
RCONH$_2$ $\rightleftharpoons$ RCN + H$_2$O	86.68	0.150

A.II   Viscosity measurements

The set-up for the viscosity measurement is shown in 38. Figure 39 provides the obtained results of the viscosity experiments. It can be seen that the viscosity of amide is higher than acid and nitrile at a temperature range of 80 to 150 °C. The obtained viscosities had an accuracy of $3 \cdot 10^{-6}$ Pa s. Moreover, Figure 39 presents that the viscosities of acid, amide and nitrile depend on the temperature.
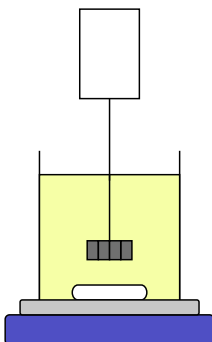
Figure 38:   Schematic overview of the viscosity experiment.

Gonzalez et al. researched two physical properties, density and viscosity, of palmitic, stearic and oleic fatty acids.[10] The obtained viscosities of the oleic acid are shown in Figure 39 at a temperature range of 25 to 150 °C. At first, it seems like the line behaves the same as the experimental data of oleic acid. Moreover, the viscosity is between the obtained experimental data of oleic acid and oleonitrile from 25 to 50 °C. But after 50 °C the viscosity decreases even more.
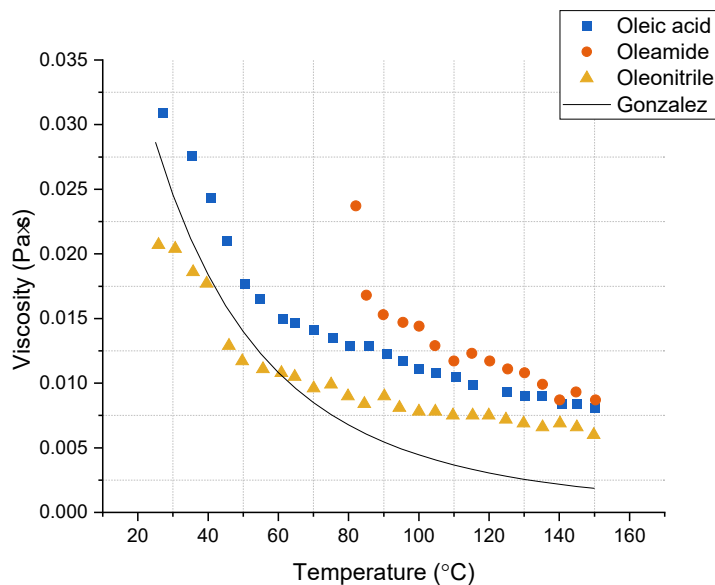
Figure 39:   Obtained viscosity of the acid, amide and nitrile at a temperature range of 25 to 150 °C.[10]

A.III   Vapor-Liquid Equilibrium

The experiments were started with high amounts of acid or nitrile and a small amount of water. Figure 40 shows the overview of the Vapor-Liquid Equilibrium (VLE) experiment. Oleic acid and oleonitrile were not soluble in water, so an emulsion was formed in the mixing chamber. The oleic components could not reach their boiling points at atmospheric pressure because the maximum temperature of the heater was 250 °C. During the experiment, only water was evaporating back into the mixing chamber. Therefore, the experiment was operated with vacuum pressure (75-78 mbar). Thus, the boiling points were approximately 250 °C at these vacuum pressures. During the experiment, the instabilities of the components were observed. There were fluctuations in the mixing chamber an as a result, the whole set-up was full of the used mixture. This also occurred when the amount of water was more than acid and nitrile. Thus, the boiling points of the acid and nitrile have never been achieved during the experiments.

After all, it is concluded that oleic acid and oleonitrile are unstable in water. During the experiments, it was only stable for a while and so the fluctuations started. Moreover, there are high differences in the boiling points of the oleic acid/water and oleonitrile/water.
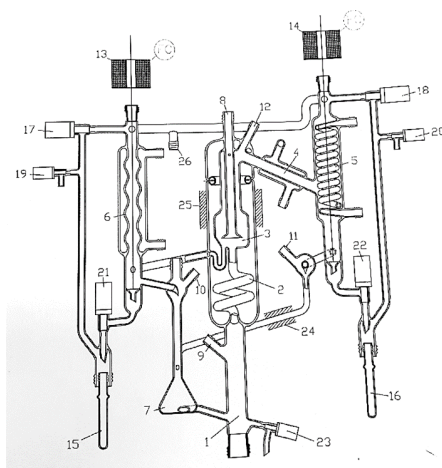
Figure 40: Schematic overview of the VLE experiment.

A.IV Matlab codes for second kinetic backward constant

Listing 1: k$_{-2}$ with Chila 5 % headspace and Mekki-Berrada et al.

```matlab
clear
clc

%% Keq determination
R = 8.314;                % Gas constant in J mol^-1 K^-1
T1 = 200+273;             % Temperature 1 in K
T2 = 300+273;             % Temperature 2 in K
n = T2-T1+1;
T = linspace(T1,T2,n);

ydata =  -17951*(1./T) + 28.847;    % Keq data with 5% headspace
xdata = T;

%% Calculation k-2
Keq = exp(ydata)';

k20_for = 12866.86691;      % pre-exponential factor in s^-1
Ea2_for = 85000;            % activation energy in J mol^-1
k2_for = k20_for*exp(-Ea2_for./(R*T))';

k2_back = (k2_for./Keq);    % kinetic constant for reaction nitrile to amide

data = [T',Keq,k2_for,k2_back];

Ea2_back = -64244.7722;     % activation energy for reaction nitrile to amide

k20_back = k2_back(101,1)/exp(-Ea2_back/(R*T(1,101)));  % obtained pre-
    exponential factor for reaction nitrile to amide at 300 C
```

Listing 2: k$_{-2}$ with Chila 5 % headspace and Appelman

```matlab
clear
clc

%% Keq determination
R = 8.314;
T1 = 200+273;                 % K
T2 = 300+273;
n = T2-T1+1;
T = linspace(T1,T2,n);

ydata = -17951*(1./T) + 28.847;
xdata = T;

%% Calculation k-2
Keq = exp(ydata)';

k20_for = 2494000000;
Ea2_for = 135439;
k2_for = k20_for*exp(-Ea2_for./(R*T))';

k2_back = (k2_for./Keq);
```

```
data = [T',Keq,k2_for,k2_back];

Ea2_back = -13805.397;

k20_back = k2_back(101,1)/exp(-Ea2_back/(R*T(1,101)));
```

Listing 3: k_{-2} with Chila 5 % headspace and Verdonk uncatalyzed

```
clear
clc

%% Keq determination
R = 8.314;
T1 = 200+273;                  % K
T2 = 300+273;
n = T2-T1+1;
T = linspace(T1,T2,n);

ydata =  -17951*(1./T) + 28.847;
xdata = T;


%% Calculation k-2
Keq = exp(ydata)';

k20_for = 1.86e11;
Ea2_for = 159600;
k2_for = k20_for*exp(-Ea2_for./(R*T))';

k2_back = (k2_for./Keq);

data = [T',Keq,k2_for,k2_back];

Ea2_back = 10355.087;

k20_back = k2_back(101,1)/exp(-Ea2_back/(R*T(1,101)));
```

Listing 4: k_{-2} with Chila 5 % headspace and Verdonk catalyzed

```
clear
clc

%% Keq determination
R = 8.314;
T1 = 200+273;                  % K
T2 = 300+273;
n = T2-T1+1;
T = linspace(T1,T2,n);

ydata =  -17951*(1./T) + 28.847;
xdata = T;


%% Calculation k-2
Keq = exp(ydata)';

k20_for = 4.66e9;
```

```
Ea2_for = 136600;
k2_for = k20_for*exp(-Ea2_for./(R*T))';

k2_back = (k2_for./Keq);

data = [T',Keq,k2_for,k2_back];

Ea2_back = -12644.7626;

k20_back = k2_back(101,1)/exp(-Ea2_back/(R*T(1,101)));
```

Listing 5: k$_{-2}$ with Chila 70 % headspace and Mekki-Berrada et al.

```
clear
clc

%% Keq determination
R = 8.314;
T1 = 200+273;                % K
T2 = 300+273;
n = T2-T1+1;
T = linspace(T1,T2,n);

ydata =  -15458*(1./T) + 12.034;
xdata = T;


%% Calculation k-2
Keq = exp(ydata)';

k20_for = 12866.86691;
Ea2_for = 85000;
k2_for = k20_for*exp(-Ea2_for./(R*T))';

k2_back = (k2_for./Keq);

data = [T',Keq,k2_for,k2_back];

Ea2_back = -43517.97020;

k20_back = k2_back(101,1)/exp(-Ea2_back/(R*T(1,101)));
```

Listing 6: k$_{-2}$ with Chila 70 % headspace and Appelman

```
clear
clc

%% Keq determination
R = 8.314;
T1 = 200+273;                % K
T2 = 300+273;
n = T2-T1+1;
T = linspace(T1,T2,n);

ydata =  -15458*(1./T) + 12.034;
xdata = T;
```

```matlab
%% Calculation k-2
Keq = exp(ydata)';

k20_for = 2494000000;
Ea2_for = 135439;
k2_for = k20_for*exp(-Ea2_for./(R*T))';

k2_back = (k2_for./Keq);

data = [T',Keq,k2_for,k2_back];

Ea2_back = 6921.15558;

k20_back = k2_back(101,1)/exp(-Ea2_back/(R*T(1,101)));
```

Listing 7: k_{-2} with Chila 70 % headspace and Verdonk uncatalyzed

```matlab
clear
clc

%% Keq determination
R = 8.314;
T1 = 200+273;              % K
T2 = 300+273;
n = T2-T1+1;
T = linspace(T1,T2,n);

ydata =  -15458*(1./T) + 12.034;
xdata = T;


%% Calculation k-2
Keq = exp(ydata)';

k20_for = 1.86e11;
Ea2_for = 159600;
k2_for = k20_for*exp(-Ea2_for./(R*T))';

k2_back = (k2_for./Keq);

data = [T',Keq,k2_for,k2_back];

Ea2_back = 31081.88900;

k20_back = k2_back(101,1)/exp(-Ea2_back/(R*T(1,101)));
```

Listing 8: k_{-2} with Chila 70 % headspace and Verdonk catalyzed

```matlab
clear
clc

%% Keq determination
R = 8.314;
T1 = 200+273;              % K
T2 = 300+273;
n = T2-T1+1;
```

```
T = linspace(T1,T2,n);


ydata =  -15458*(1./T) + 12.034;
xdata = T;



%% Calculation k-2
Keq = exp(ydata)';

k20_for = 4.66e9;
Ea2_for = 136600;
k2_for = k20_for*exp(-Ea2_for./(R*T))';

k2_back = (k2_for./Keq);

data = [T',Keq,k2_for,k2_back];

Ea2_back = 8082.20568;

k20_back = k2_back(101,1)/exp(-Ea2_back/(R*T(1,101)));
```

Listing 9: k$_{-2}$ with DFT and Mekki-Berrada et al.

```
clear
clc

%% delta G for each temperature
d_H2 = 86.68e3;          % Enthalpy in J mol^-1
d_S2 = 0.149890994e3;    % Entropy in J mol^-1

R  = 8.314;              % Gas constant in J mol^-1 K^-1
T1 = 200+273;            % Temperature 1 in K
T2 = 300+273;            % Temperature 2 in K
n = T2-T1+1;
T = linspace(T1,T2,n);

d_G2 = d_H2 - T*d_S2;    % Calculation of Gibbs energy in J mol^-1

lnK2 = -d_G2 ./ (R*T);

K2= exp(lnK2);           % Calculation of Keq,2

%% Calculation k-2
Keq = K2;

k20_for = 12866.86691;                    % pre-exponential factor in s^-1
Ea2_for = 85000;                          % activation energy in J mol^-1
k2_for = k20_for*exp(-Ea2_for./(R*T));

k2_back = (k2_for./Keq);                  % kinetic constant for reaction
    nitrile to amide

data = [T',Keq',k2_for',k2_back'];

Ea2_back = -1680.00998;                   % activation energy for reaction
    nitrile to amide
```

```
k20_back = k2_back(1,101)/exp(-Ea2_back/(R*T(1,101))); % obtained pre-
    exponential factor for reaction nitrile to amide at 300 C
```

Listing 10: k_{-2} with DFT and Appelman

```
clear
clc

%% delta G for each temperature
d_H2 = 86.68e3;
d_S2 = 0.149890994e3;

R  = 8.314;
T1 = 200+273;              % K
T2 = 300+273;
n = T2-T1+1;
T = linspace(T1,T2,n);

d_G2 = d_H2 - T*d_S2;

lnK2 = -d_G2 ./ (R*T);

K2= exp(lnK2);

%% Calculation k-2
Keq = K2;

k20_for = 2494000000;
Ea2_for = 135439;
k2_for = k20_for*exp(-Ea2_for./(R*T));

k2_back = (k2_for./Keq);

data = [T',Keq',k2_for',k2_back'];

Ea2_back = 48759.1158;

k20_back = k2_back(1,101)/exp(-Ea2_back/(R*T(1,101)));
```

Listing 11: k_{-2} with DFT and Verdonk uncatalyzed

```
clear
clc

%% delta G for each temperature
d_H2 = 86.68e3;
d_S2 = 0.149890994e3;

R  = 8.314;
T1 = 200+273;              % K
T2 = 300+273;
n = T2-T1+1;
T = linspace(T1,T2,n);

d_G2 = d_H2 - T*d_S2;

lnK2 = -d_G2 ./ (R*T);
```

```matlab
K2= exp(lnK2);

%% Calculation k-2
Keq = K2;

k20_for = 1.86e11;
Ea2_for = 159600;
k2_for = k20_for*exp(-Ea2_for./(R*T));

k2_back = (k2_for./Keq);

data = [T',Keq',k2_for',k2_back'];

Ea2_back = 72919.5998;

k20_back = k2_back(1,101)/exp(-Ea2_back/(R*T(1,101)));
```

Listing 12: k_{-2} with DFT and Verdonk catalyzed

```matlab
clear
clc

%% delta G for each temperature
d_H2 = 86.68e3;
d_S2 = 0.149890994e3;

R  = 8.314;
T1 = 200+273;               % K
T2 = 300+273;
n = T2-T1+1;
T = linspace(T1,T2,n);

d_G2 = d_H2 - T*d_S2;

lnK2 = -d_G2 ./ (R*T);

K2= exp(lnK2);

%% Calculation k-2
Keq = K2;

k20_for = 4660000000;
Ea2_for = 136600;
k2_for = k20_for*exp(-Ea2_for./(R*T));

k2_back = (k2_for./Keq);

data = [T',Keq',k2_for',k2_back'];

Ea2_back = 49919.7502;

k20_back = k2_back(1,101)/exp(-Ea2_back/(R*T(1,101)));
```

A.V   Matlab script: Coefficients of the Henry components

Listing 13: Henry component NH$_3$

```matlab
clear
clc

%% Input data

file = readtable('Data_henryNH3.xlsx'); % data Henry component NH3

xdata = table2array(file(:,2));

H_NH3_ac = table2array(file(:,3));
H_NH3_am = table2array(file(:,4));
H_NH3_nit = table2array(file(:,5));

y_NH3_ac = log(H_NH3_ac);          % ln H
y_NH3_am = log(H_NH3_am);
y_NH3_nit = log(H_NH3_nit);

fun1 = @(x) x(1)+ (x(2)./xdata) + (x(3)*log(xdata)) + (x(4)*xdata) - y_NH3_ac;
fun2 = @(x) x(1)+ (x(2)./xdata) + (x(3)*log(xdata)) + (x(4)*xdata) - y_NH3_am;
fun3 = @(x) x(1)+ (x(2)./xdata) + (x(3)*log(xdata)) + (x(4)*xdata) - y_NH3_nit
    ;

x0 = linspace(-1e5,1e5,4);
options = optimoptions('lsqnonlin','Display','iter');

x1 = lsqnonlin(fun1,x0,[],[],options);
x2 = lsqnonlin(fun2,x0,[],[],options);
x3 = lsqnonlin(fun3,x0,[],[],options);
%% Values A, B, C, D for equation ln(H)

A_ac = x1(1,1);                    % Coefficient A for NH3 in acid
B_ac = x1(1,2);                    % Coefficient B for NH3 in acid
C_ac = x1(1,3);                    % Coefficient C for NH3 in acid
D_ac = x1(1,4);                    % Coefficient D for NH3 in acid
list1 = [A_ac;B_ac;C_ac;D_ac]';

A_am = x2(1,1);
B_am = x2(1,2);
C_am = x2(1,3);
D_am = x2(1,4);
list2 = [A_am;B_am;C_am;D_am]';

A_nit = x3(1,1);
B_nit = x3(1,2);
C_nit = x3(1,3);
D_nit = x3(1,4);
list3 = [A_nit;B_nit;C_nit;D_nit]';
```

Listing 14: Henry component H$_2$O

```matlab
clear
clc
```

```matlab
%% Input data

file = readtable('Data_henryH2O.xlsx'); % data Henry component H2O

xdata = table2array(file(:,2));

H_H2O_ac = table2array(file(:,3));
H_H2O_am = table2array(file(:,4));
H_H2O_nit = table2array(file(:,5));

y_H2O_ac = log(H_H2O_ac);
y_H2O_am = log(H_H2O_am);
y_H2O_nit = log(H_H2O_nit);

fun1 = @(x) x(1)+ (x(2)./xdata) + (x(3)*log(xdata)) + (x(4)*xdata) - y_H2O_ac;
fun2 = @(x) x(1)+ (x(2)./xdata) + (x(3)*log(xdata)) + (x(4)*xdata) - y_H2O_am;
fun3 = @(x) x(1)+ (x(2)./xdata) + (x(3)*log(xdata)) + (x(4)*xdata) - y_H2O_nit
    ;

x0 = linspace(-1e5,1e5,4);
options = optimoptions('lsqnonlin','Display','iter');

x1 = lsqnonlin(fun1,x0,[],[],options);
x2 = lsqnonlin(fun2,x0,[],[],options);
x3 = lsqnonlin(fun3,x0,[],[],options);
%% Values A, B, C, D for equation ln(H)

A_ac = x1(1,1);
B_ac = x1(1,2);
C_ac = x1(1,3);
D_ac = x1(1,4);
list1 = [A_ac;B_ac;C_ac;D_ac]';

A_am = x2(1,1);
B_am = x2(1,2);
C_am = x2(1,3);
D_am = x2(1,4);s
list2 = [A_am;B_am;C_am;D_am]';

A_nit = x3(1,1);
B_nit = x3(1,2);
C_nit = x3(1,3);
D_nit = x3(1,4);
list3 = [A_nit;B_nit;C_nit;D_nit]';
```

A.VI   Set-up simulations in Aspen
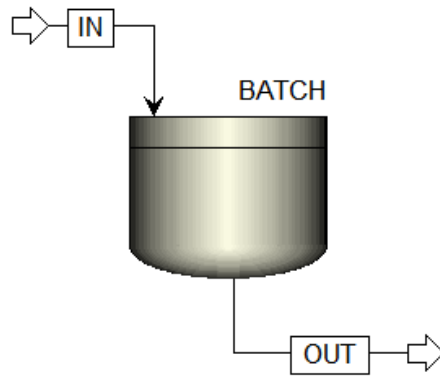
Figure 41: Set-up for the Batch in Aspen.
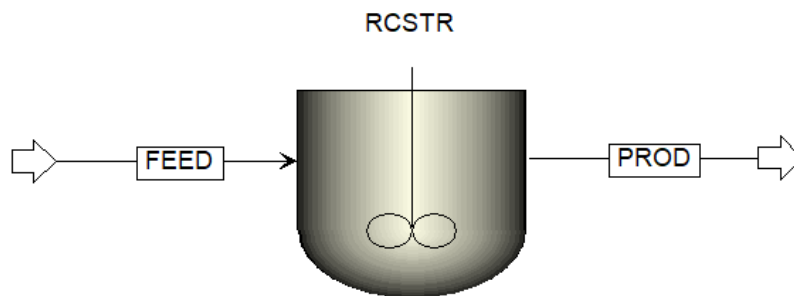
Figure 42: Set-up for the CSTR in Aspen.
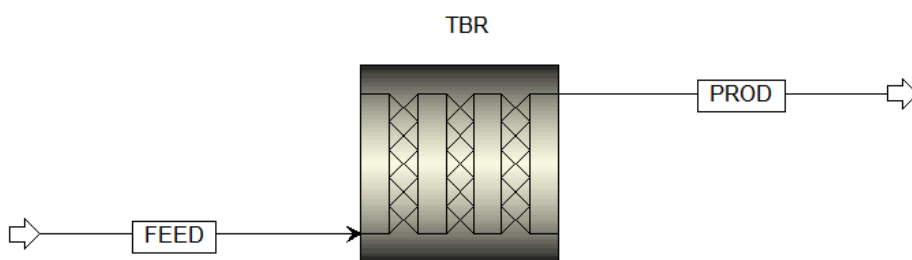
Figure 43: Set-up for the TBR in Aspen.
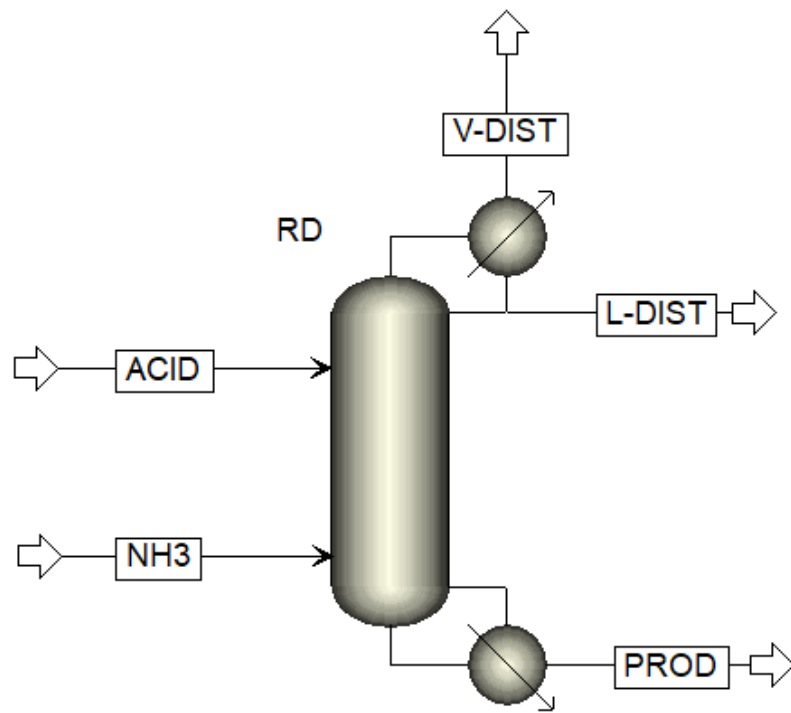
Figure 44: Set-up for the RDC in Aspen.

A.VII   Pressure experiment with autoclaves

To measure the pressure in the autoclaves, the same set-up was used as Figure 13 at a temperature of 300 °C for 5 h. This time with a pressure meter on top of the autoclave. The reactants were oleonitrile and demi-water with mass amounts of 1.56 and 3.58 g, respectively. So, there was only headspace between the top of the autoclave and the bottom part of the pressure meter. Thus, a volume ratio of 1:2 nitrile to water was used. Excess of water caused separate phases as a product, a nitrile layer and a water layer. A possible explanation for this might be the solubility of the water in nitrile. This can be seen in Figure 12b where Henry's law constant is very low over temperature for water in nitrile.

Figure 45: Autoclave with a pressure meter used for measuring the pressures.

The obtained temperatures of the experiment are shown in Figure 46 over time. It can be seen that there is instability in the process because of the fluctuations in the data. Moreover, the obtained pressures are shown in Figure 47. From this graph, it can be seen that the pressure is also unstable. An explanation for this can be the high amount of water present in the autoclaves. Water is in the vapor phase at 300 °C, so it can be that this component is unstable during the process. All in all, the obtained pressures are approximately 60 bar in the autoclaves during the experiments - using oleonitrile and demi-water as reactants.
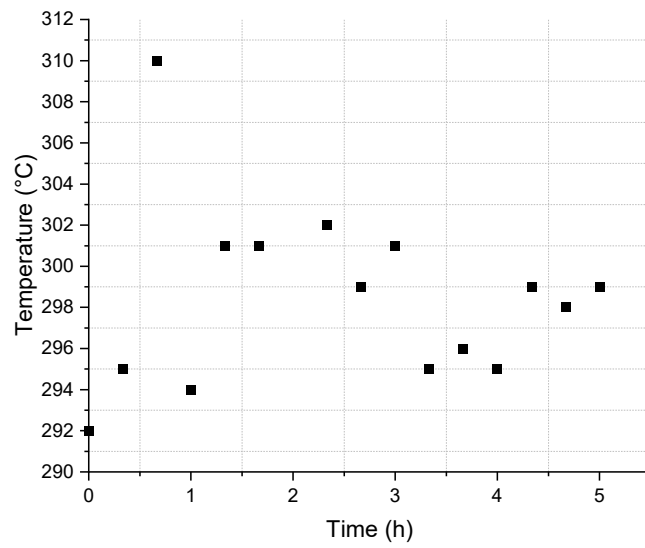
Figure 46: Obtained results from the pressure experiment; temperatures in °C over time in h.
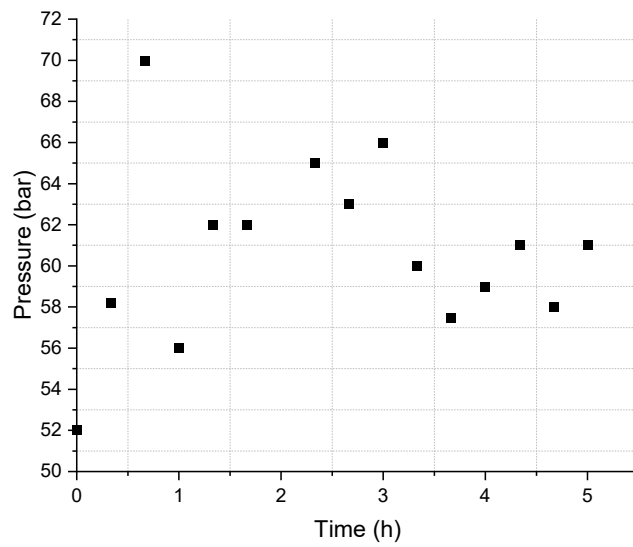
Figure 47: Obtained results from the pressure experiment; pressures in bar over time in h.

A.VIII   Results Batch autoclave exp

The outgoing batch products acid, amide and nitrile from Chila 5 % are shown in Figure 48. Simulation 1, from experiments 1 to 3, is fitting with the mole compositions obtained from experimental results. However, there is more acid and less nitrile formation in experiments 4 to 6. The other simulations 2 to 4 do not fit with the experimental results, less amide and a lot of acid formation were detected. There was a significant difference between Chila 5 % with and without adding Henry's law components, by adding these components there was more formation of amide detected (see Figure 49). As a result, none of the simulations are fitting with the experimental data.

(a) Experiment 1.
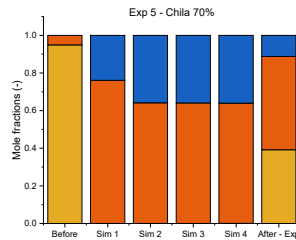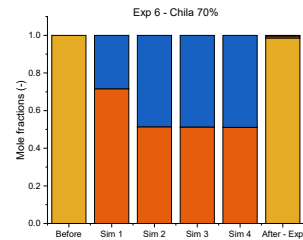
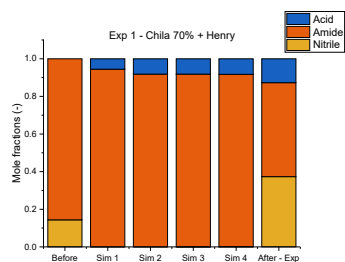(b) Experiment 2.

(c) Experiment 3.
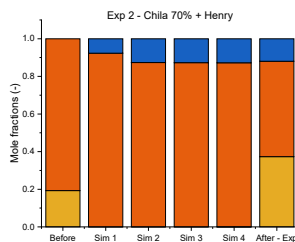
(d) Experiment 4.

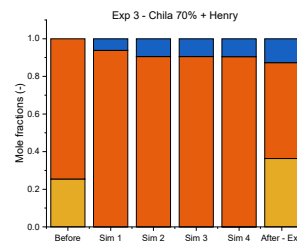(e) Experiment 5.
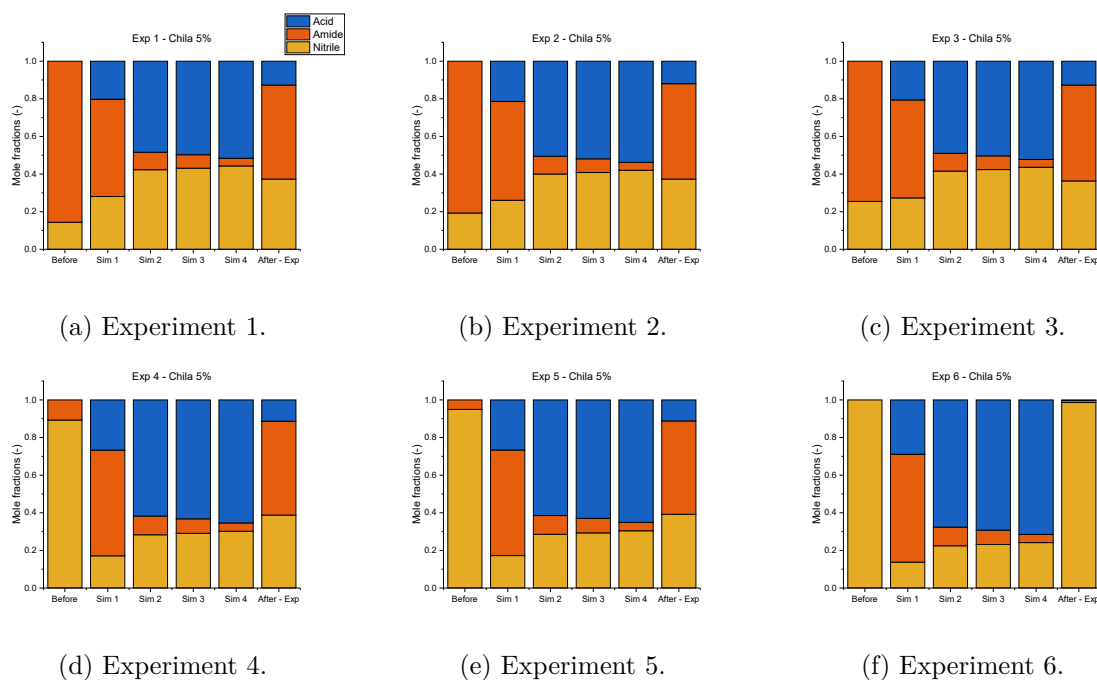
(f) Experiment 6.

Figure 48: Mole compositions in the liquid phase of acid, amide and nitrile of experiments 1-6; From left to right: mole compositions before experiment and simulation, simulation 1, 2, 3 and 4 followed by the experimental result at $t_R = 5$ h; Simulations 1-4 used Chila with 5 % headspace equilibrium data.[8]
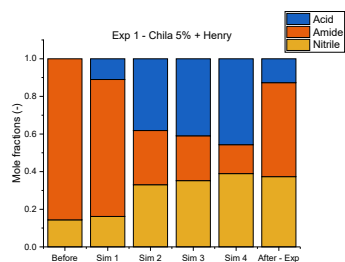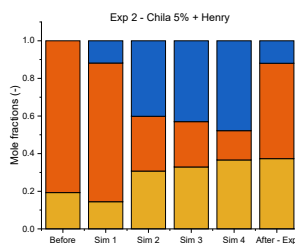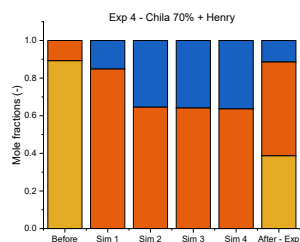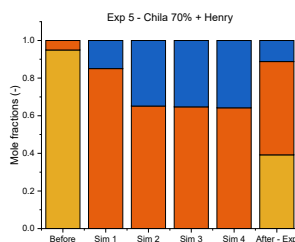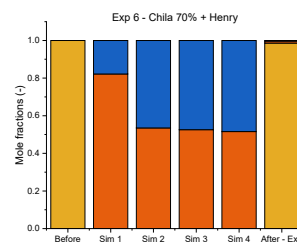
(a) Experiment 1.   (b) Experiment 2.   (c) Experiment 3.
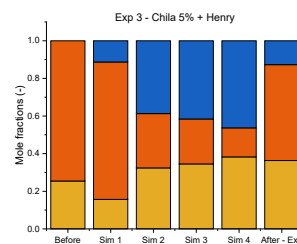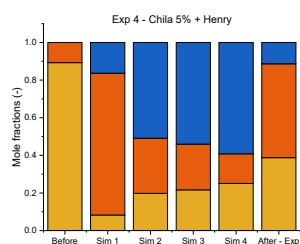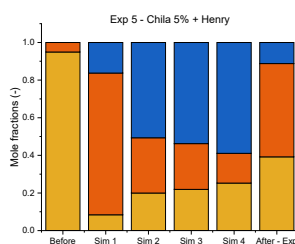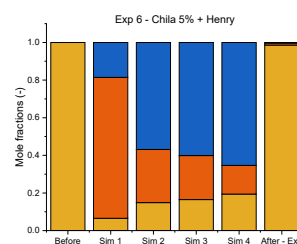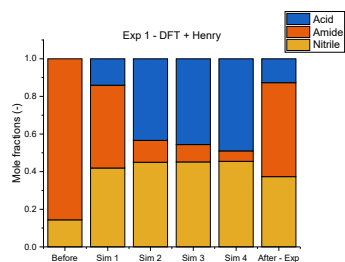
(d) Experiment 4.   (e) Experiment 5.   (f) Experiment 6.

Figure 49: Mole compositions in the liquid phase of acid, amide and nitrile of experiments 1-6; From left to right: mole compositions before experiment and simulation, simulation 1, 2, 3 and 4 followed by the experimental result at $t_R = 5$ h; Simulations 1-4 used Chila with 5 % headspace equilibrium data and Henry constants.[8,9]

Next, kinetic data from Chila with 70 % headspace resulted in the following batch compositions in Figure 50. Surprising that using more headspace in the batch reactor results in no nitrile formation. No single simulation matches the experimental data. Moreover, there is little to no difference when Henry components are added to the process. This can be seen in Figure 51.
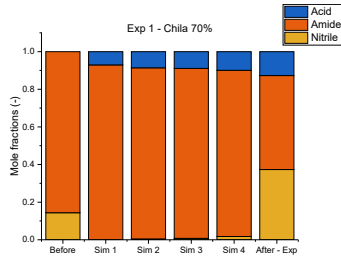
(a) Experiment 1.
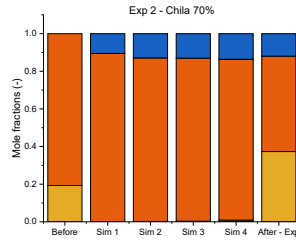
(b) Experiment 2.
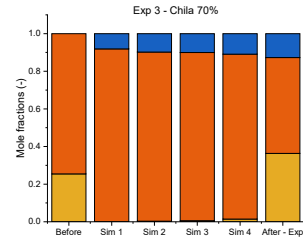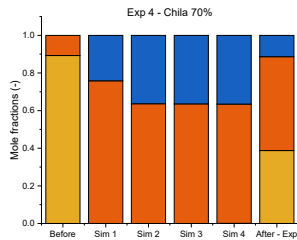
(c) Experiment 3.

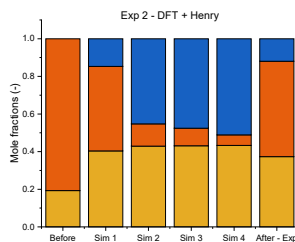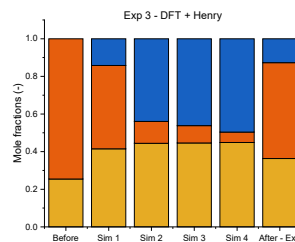(d) Experiment 4.

(e) Experiment 5.

(f) Experiment 6.

Figure 50: Mole compositions in the liquid phase of acid, amide and nitrile of experiments 1-6; From left to right: mole compositions before experiment and simulation, simulation 1, 2, 3 and 4 followed by the experimental result at $t_R = 5$ h; Simulations 1-4 used Chila with 70 % headspace equilibrium data.[8]
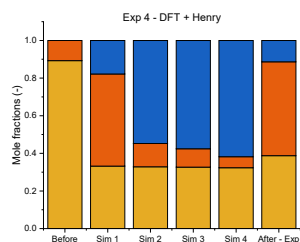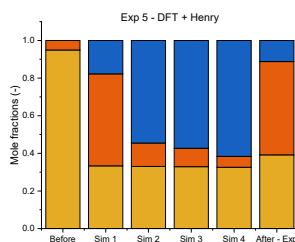
(a) Experiment 1.

(b) Experiment 2.

(c) Experiment 3.

(d) Experiment 4.

(e) Experiment 5.

(f) Experiment 6.

Figure 51: Mole compositions in the liquid phase of acid, amide and nitrile of experiments 1-6; From left to right: mole compositions before experiment and simulation, simulation 1, 2, 3 and 4 followed by the experimental result at $t_R = 5$ h; Simulations 1-4 used Chila with 70 % headspace equilibrium data and Henry constants.[8,9]
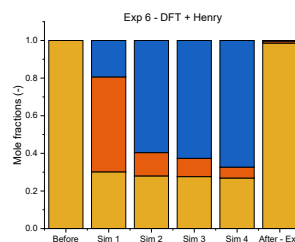
(a) Experiment 1.

(b) Experiment 2.

(c) Experiment 3.

(d) Experiment 4.

(e) Experiment 5.

(f) Experiment 6.

Figure 52: Mole compositions in the liquid phase of acid, amide and nitrile of experiments 1-6; From left to right: mole compositions before experiment and simulation, simulation 1, 2, 3 and 4 followed by the experimental result at $t_R = 5$ h; Simulations 1-4 used DFT equilibrium data and Henry constants.[9]
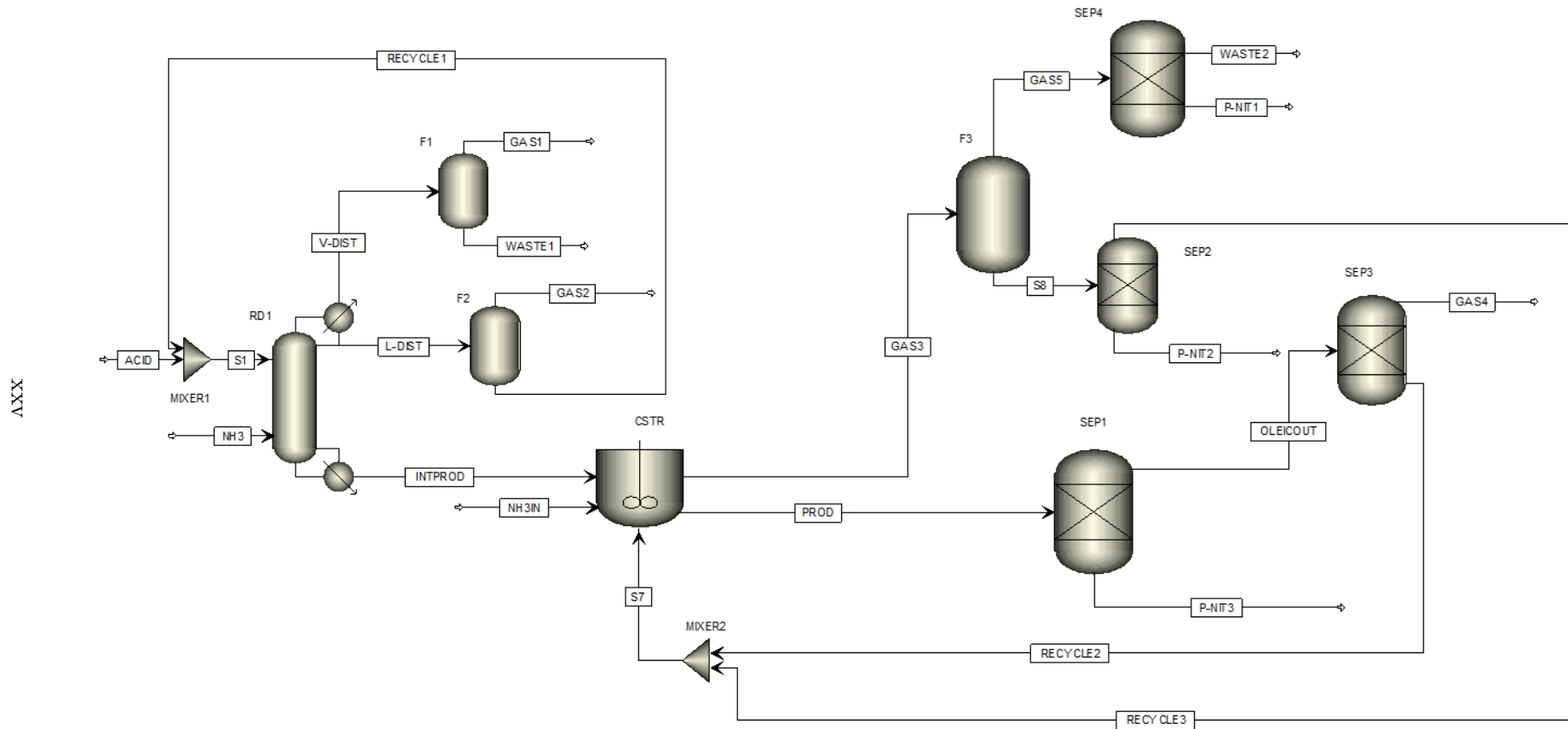
Figure 53: Set-up for the developed model 4 in Aspen.